Broadband High-Fidelity Directional Transient Couplers

by

Micah Stickel

September 1999

A thesis submitted in conformity with the requirements
for the degree of Master of Applied Science
Graduate Department of Electrical and Computer Engineering
University of Toronto

Broadband High-Fidelity Directional Transient Couplers

Micah Stickel

Master of Applied Science
Graduate Department of Electrical and Computer Engineering
University of Toronto
1999

ABSTRACT

A review of coupling theory is compiled with specific emphasis on the mechanisms present in a resistive directional coupler (RDC). An improved theoretical model for an RDC is developed, which can aid in the synthesis of more complicated designs than was allowed by a previously published model. With the use of this model, a general design procedure for an RDC is presented. Couplers for both stripline and microstrip environments are synthesized and their theoretical performances are validated with the use of commercially available electromagnetic simulators.

ACKNOWLEDGEMENTS

I would like to express my sincerest appreciation for the guidance and support that Professor Balmain has provided during the course of this research. His thoughtful consideration, rooted in the fundamentals of electromagnetic theory, will always be a virtue to aspire to. I also thank the many friends, Ramesh Abhari, Peter Aaen, Karam Noujeim, Leesa Noujeim, Mina Danesh, Xidong Wu, and the other members of the Electromagnetics Group who have given me advice and assistance throughout this project. Finally, to my parents Richard and Alicia, my sister Shone, and Elizabeth, I cannot thank you enough for your kindness, consideration, and support.

The research that led to this thesis was supported by Nortel Networks and the NSERC/Bell Canada/Nortel Industrial Research Chair in Electromagnetics and the Natural Sciences and Engineering Research Council.

TABLE OF CONTENTS

LIST OF FIGURES

Chapter 1

INTRODUCTION

Since the advent of the directional coupler in the early 1940s, there has been much work done in analyzing, designing and finding new applications for these structures. One of the most common forms of this device consists of two or more parallel-coupled transmission lines. Usually the lines are placed in close proximity to each other and the interaction of the fields surrounding the lines provides the coupling path. In some couplers, such as with the well-known branch line coupler, the coupling occurs through the direct connection of the two main lines. The resistive directional coupler (RDC) that is the focus of this thesis is a combination of these two types of couplers where both direct, or DC coupling, and electromagnetic (EM) coupling is considered.

It was observed very early on in the development of the directional coupler how useful this device could be to all areas of microwave technology. Because of this, much information has been published over the past 50 years concerning directional couplers. The book edited by Leo Young [1] in 1972 provides an excellent outline of the fundamentals of coupler theory and design. Almost every type of coupler constructed from parallel-coupled lines is discussed and design data and procedures are presented. More recently, there have been many books that have included modern developments of parallel-coupled-line directional couplers.

However, there has been very little information published pertaining to coupler designs that are suitable for digital systems. These systems require devices that can operate over large bandwidths due to the fact that pulses are the signals being used. Traditionally, directional couplers are designed to work at a single frequency or over a specified bandwidth.

However, the wideband nature of directional couplers is constantly improving as new topologies and manufacturing techniques are being employed. This has been proved recently when a 20 dB coupler that operates from 10 – 60 GHz was developed using micromachining techniques [2]. Nevertheless, the performance of wideband directional couplers in terms of the pulse propagation that occurs in digital systems has not been considered.

If one examines the time-domain response of a parallel-coupled-line directional coupler, one will find that all the information held within the pulse is not transferred. As an example, the performance of a microstrip directional coupler, which has the geometry shown in Fig. 1-1, will be examined. Specifically, the time-domain response for this coupler is shown in Fig. 1-2. Due to the fact that there is no direct connection between the main lines, the DC characteristic, i.e., the flat top, of the pulse is lost. This results in a coupled signal that only represents the edges of the input pulse rather than the pulse in its entirety. Clearly, this is not the ideal performance for a directional coupler in a digital system. Therefore, there is a need for directional couplers that have been specifically designed for use in digital systems.

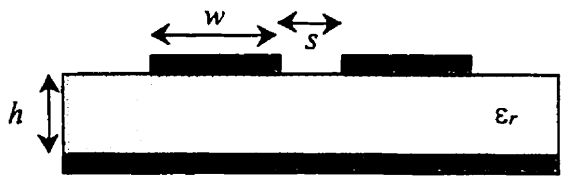

Figure 1-1. Design parameters of a microstrip edge-to-edge directional coupler: L is the length of the lines.

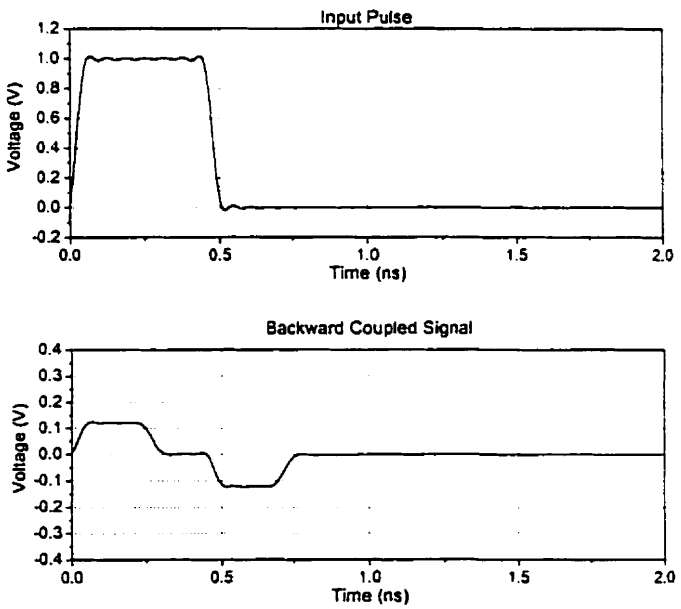

Figure 1-2. Input pulse and coupled output pulse for a microstrip edge-to-edge coupler. (w=0.62mm, h=0.635mm, s=0.3mm, ε_r=9.8, L=14.38mm)

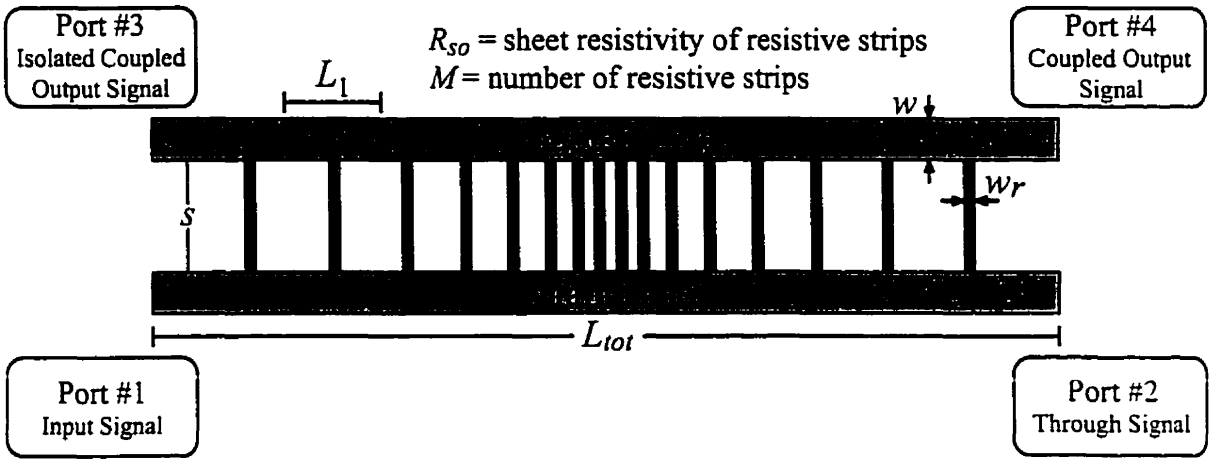

Figure 1-3. General topology of the resistive directional coupler: h is the height of the traces above ground.

It was the focus of this research to apply the concept of an RDC, which was first proposed by Jenkins and Cullen in 1982 [3], to design a directional transient coupler that provides a high level of pulse fidelity. The general topology, the design parameters, and the port definitions of an RDC are shown in Fig. 1-3. In this coupler design, the resistive strips that connect the two main lines provide the path for the DC characteristics of the pulses to be transferred. In addition, directional qualities can be achieved over a wide bandwidth, which results in significant isolation while maintaining excellent reproduction of the input pulse at the coupled output port.

The goal of this thesis is to present a thorough study of the theory and design of an RDC and how it can be applied to the high-fidelity transmission of rectangular pulses. The essential elements of coupling theory will be reviewed in Chapter 2. Specifically, the physical mechanisms, and their associated mathematical formulations, that lead to coupling in the backward and forward directions along two parallel-coupled lines will be discussed. This information will be useful in understanding the performance of both stripline and microstrip RDCs. In Chapter 3, the methods of analysis of the RDC designs will be presented. This includes the development of a theoretical model and the introduction to the

EM simulators that were used to verify the results of the model. Finally, a design procedure for an RDC will be proposed and then applied to three specific coupler designs that have various degrees of coupling, directivity and pulse fidelity.

Chapter 2

COUPLING THEORY

To investigate the resistive directional coupler, the fundamentals of coupling between two parallel transmission lines must first be introduced. Coupled-mode theory will be used to determine expressions for the possible waves travelling along two coupled lines. These expressions will provide insight into the mechanisms of coupling and in particular they will highlight the existence of the directionality of coupling, namely forward and backward coupling.

2.1. Coupled Transmission Line Analysis

The analysis of coupled transmission lines can be approached in the same way as the analysis of a single transmission line. First, a set of differential equations that completely describe the voltage and current behavior along the lines can be derived from a lumped equivalent circuit. Second, the propagation constants of the propagating waves are then found by solving the set of differential equations.

To determine this set of differential equations, the equivalent circuit of the coupled lines must be examined. The coupled lines, with their respective voltage and current definitions, along with their equivalent circuit are shown in Fig. 2-1. From this circuit, the equations for two coupled lossless lines can be written as [4]

$$\frac{\partial v_1}{\partial z} = -L_{11}\frac{\partial i_1}{\partial t} - L_m\frac{\partial i_2}{\partial t} \tag{2-1}$$

$$\frac{\partial i_1}{\partial z} = -C_{11}\frac{\partial v_1}{\partial t} + C_m\frac{\partial v_2}{\partial t} \tag{2-2}$$

$$\frac{\partial v_2}{\partial z} = -L_{22}\frac{\partial i_2}{\partial t} - L_m\frac{\partial i_1}{\partial t} \tag{2-3}$$

$$\frac{\partial i_2}{\partial z} = -C_{22}\frac{\partial v_2}{\partial t} + C_m\frac{\partial v_1}{\partial t} \tag{2-4}$$

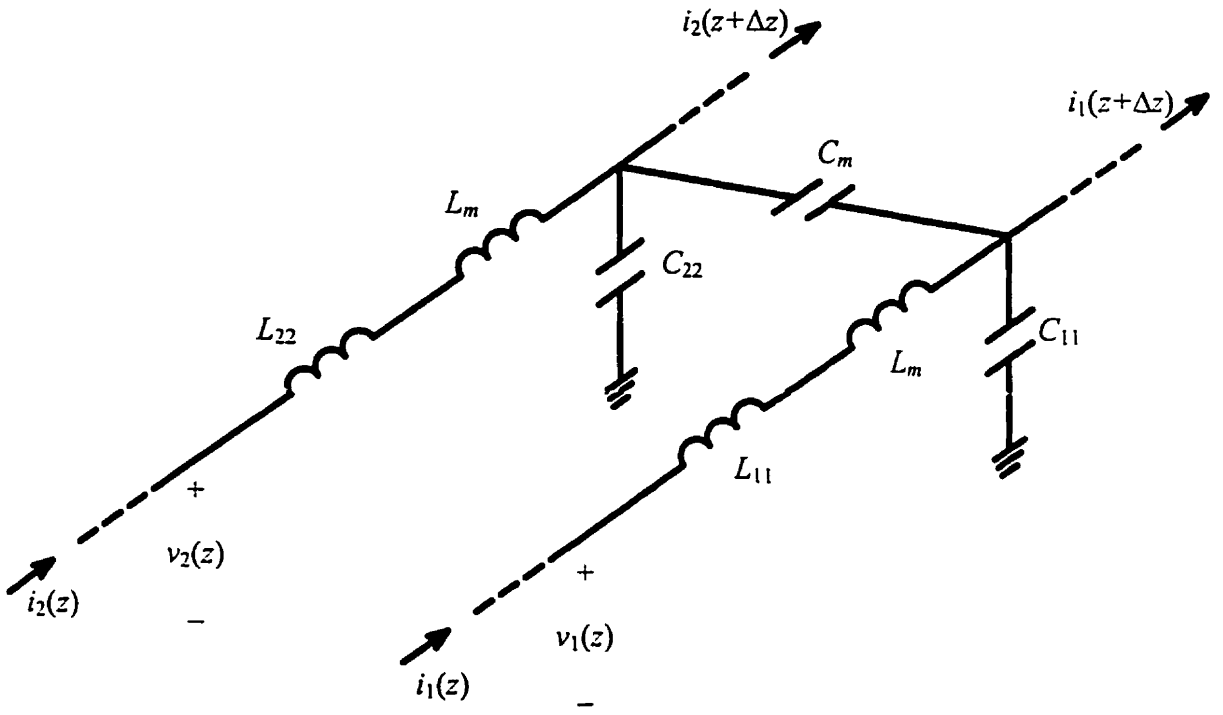

Figure 2-1. Equivalent circuit of two coupled transmission lines.

where L_m and C_m are the mutual inductance and capacitance per unit length between the two lines, and L_{ii} and C_{ii} are the self-inductance and self-capacitance per unit length of line i (i=1,2) in the presence of line j (j=1,2, $j \neq i$). It should be noted that linear, isotropic media have been assumed, which means that $L_{12} = L_{21} = L_m$ and $C_{12} = C_{21} = C_m$. Also, for the case of lines with transverse symmetry, i.e., lines with the same geometry, $L_{11} = L_{22}$ and $C_{11} = C_{22}$.

2.1.1. Coupled-Mode Formulation

To gain a more intuitive understanding of how the mechanisms of coupling work along the transmission lines, eqs. (2-1) – (2-4) can be re-written in terms of wave parameters as opposed to voltages and currents. To achieve this, the following definitions can be used to characterize the modes travelling along line 1 [5]

$$a_{\pm}(z,t) = a_{\pm}(z)e^{j\omega t} = \frac{1}{2\sqrt{Z_1}}(v_1 \pm Z_1 i_1) \tag{2-5}$$

and along line 2

$$b_{\pm}(z,t) = b_{\pm}(z)e^{j\omega t} = \frac{1}{2\sqrt{Z_2}}(v_2 \pm Z_2 i_2) \tag{2-6}$$

In these equations $Z_i = \sqrt{L_{ii}/C_{ii}}$ (i=1,2), representing the characteristic impedance of line i in the presence of the other line. The complex wave amplitudes $a_{\pm}(z)$ and $b_{\pm}(z)$ represent both the magnitude and phase characteristics of the forward (+ sign) and backward (– sign) travelling waves on each line. They have been normalized such that, for instance, $|a_{+}(z)|^2/2$ is the power flow in the positive direction along line 1.

If (2-5) and (2-6) are rearranged and then substituted into (2-1) – (2-4) the set of differential equations can be cast into a coupled-mode form. Before the results of this substitution are presented it is necessary to introduce some important parameters. First, $\beta_i = \omega\sqrt{L_{ii}C_{ii}}$ (i=1,2) is the propagation constant of a wave travelling along line i in the presence of the other line and for symmetric lines, β_1 and β_2 will be equal. Two other parameters of interest are the inductive and capacitive coupling coefficients, which are defined as [5]

$$k_L = \frac{L_m}{\sqrt{L_{11}L_{22}}} \tag{2-7}$$

$$k_C = \frac{C_m}{\sqrt{C_{11}C_{22}}} \tag{2-8}$$

These coefficients are very commonly used in directional coupler design and quantitatively characterize the amount of coupling present. It will be seen below how important these parameters are in determining what type of coupling is present.

With these parameters in mind, and if it is assumed that the line impedances (Z_1 and Z_2) do not vary with distance z, then the coupled-mode equations can be simplified to [5]

$$\left(\pm j\beta_1 + \frac{\partial}{\partial z}\right) a_{\pm}(z) = -j\sqrt{\beta_1\beta_2}\left[\left(\frac{k_L \mp k_C}{2}\right) b_{+} - \left(\frac{k_L \pm k_C}{2}\right) b_{-}\right] \tag{2-9}$$

$$\left(\pm j\beta_2 + \frac{\partial}{\partial z}\right) b_{\pm}(z) = -j\sqrt{\beta_1\beta_2}\left[\left(\frac{k_L \mp k_C}{2}\right) a_{+} - \left(\frac{k_L \pm k_C}{2}\right) a_{-}\right] \tag{2-10}$$

These equations are very general in their nature, in fact the only assumptions that have been made are that the lossless lines exist in a linear and isotropic medium and that the individual characteristic impedances of the lines remain constant along the length of the coupler. This means that they are applicable to both stripline and microstrip environments. For the lines where Z_1 and Z_2 vary with distance, Adair and Haddad present similar coupled-mode equations in [6]. It can be seen from (2-9) and (2-10) how the various modes travelling along the lines couple to one another depending on the relative values of k_C and k_L. There are some specific cases of interest and they will be discussed in further detail later.

With these equations it is then possible to solve for the wave propagation constants by assuming an $a(z) = a_0 e^{\gamma z}$ variation with distance for each of the four modes. With this assumption the solution for the propagation constants takes the form [5]

$$\gamma = \pm\beta_0\sqrt{1 \pm \delta^2} \tag{2-11a}$$

where

$$\beta_0 = \sqrt{\frac{\beta_1^2 + \beta_2^2}{2} - \beta_1\beta_2 k_L k_C} \tag{2-11b}$$

and

$$\delta = \sqrt{1 - \left(\frac{\beta_1^2\beta_2^2}{\beta_0^4}\right)\left(1 - k_L^2\right)\left(1 - k_C^2\right)} \tag{2-11c}$$

From (2-11a), it can be seen that there are four possible waves that can be present within the coupler, one in each direction for both lines.

2.1.2. Even and Odd Mode Formulation

The even and odd mode analysis of couplers is by far the most common due its ease of application and clarity of its solutions. Essentially, it is a specific case of the coupled-mode formulation where the two modes are defined in such a way that they propagate independently of each other. The only requirement for such modes to exist is that the lines be identical, and this condition will be assumed to be true for the remainder of this section. However, it is possible to identify two independently propagating modes for asymmetric lines if $L_{11}\ C_{11} = L_{22}\ C_{22}$ and the characteristic impedances of the two lines are related by a constant ratio [7].

The even and odd mode formulation can be derived in the same manner as the coupled-mode formulation with the only difference being that the voltages and currents for each line are replaced with voltages and currents for each mode. Indeed, they can be written as

$$v_e = \frac{v_1 + v_2}{2} \tag{2-12a}$$

$$i_e = \frac{i_1 + i_2}{2} \tag{2-12b}$$

$$v_o = \frac{v_1 - v_2}{2} \tag{2-12c}$$

$$i_o = \frac{i_1 - i_2}{2} \tag{2-12d}$$

These definitions lead to two possible "excitations" of the coupled lines. For the even mode, both lines are excited with equal voltages of the same polarity, which cause the line currents to flow in the same direction. For the odd mode, the lines are excited with equal voltages of opposite polarity, which cause the line currents to oppose each other.

Continuing with the coupled-mode formulation, the mode amplitudes can be defined as

$$a_{e\pm} = \frac{1}{2\sqrt{Z_{0e}}}(v_e \pm Z_{0e} i_e) \tag{2-13}$$

$$a_{o\pm} = \frac{1}{2\sqrt{Z_{0o}}}(v_o \pm Z_{0o} i_o) \tag{2-14}$$

where the even and odd mode characteristic impedances are given by [6]

$$Z_{0e} = \sqrt{\frac{L_{10}}{C_{10}}} = Z_{10} \tag{2-15}$$

$$Z_{0o} = Z_{0e}\sqrt{\frac{(1-k_L)}{(1+k_L)}\frac{(1-k_C)}{(1+k_C)}} \tag{2-16}$$

and the coupled-mode equations become

$$\frac{da_{e\pm}}{dz} = \mp j\beta_e a_{e\pm} \tag{2-17}$$

$$\frac{da_{o\pm}}{dz} = \mp j\beta_o a_{o\pm} \tag{2-18}$$

where it has again been assumed that the line characteristic impedances do not vary with z. The two propagation constants are defined to be [6]

$$\beta_e = \omega\sqrt{L_{10}C_{10}} = \frac{\omega}{c} \tag{2-19}$$

$$\beta_o = \frac{\omega}{c}\sqrt{\left(\frac{1-k_L}{1+k_L}\right)\left(\frac{1-k_C}{1+k_C}\right)} \tag{2-20}$$

Equation (2-19) indicates that the even mode propagates as it would along a solitary line travelling at the speed of light c within the surrounding medium. On the other hand, if $k_L \neq k_C$, the odd mode travels with a phase velocity that is larger than v_e. In the design of microstrip RDCs, this difference in phase velocities will prove to pose a challenging

problem. It should also be noted that by examining (2-17) and (2-18) it can be seen that $a_{e\pm}$ does not depend on $a_{o\pm}$ at all, proving the independence of the two modes.

2.1.3. Backward Coupling

Backward, or contra-directional coupling is defined as the case in which the coupled signal travels in a direction that is opposite to the propagation of the input signal, i.e., the coupled output signal exits port #3 for a signal input at port #1. To gain insight into the physical mechanisms that lead to backward coupling, a small elemental coupled section will first be analyzed. Then the existence of backward coupling will be derived as a special case of the coupled-mode formulation.

2.1.3.1. Coupled Elemental Length of Line

The process of backward coupling can best be illustrated by examining the voltage and current characteristics of a weakly coupled short section of coupled lines. For the configuration shown in Fig. 2-2, the input wave travels from left to right along line 1. This line will be assumed to be well-matched, meaning there is no wave travelling from right to left along line 1. As the input wave changes in time, an inductive voltage and a capacitive current will be excited on line 2. These incremental values can be written as

$$i_C = C_m \frac{dv_1}{dt} \tag{2-21}$$

$$v_L = L_m \frac{di_1}{dt} \tag{2-22}$$

Upon examination of two of the original differential equations, (2-3) and (2-4), it seems that i_C and v_L do not fully describe the current and voltage on line 2. However, because weak coupling is assumed, i.e., i_2 and v_2 are very small, the effects of v_2 on i_2, and i_2 on v_2 can be neglected.

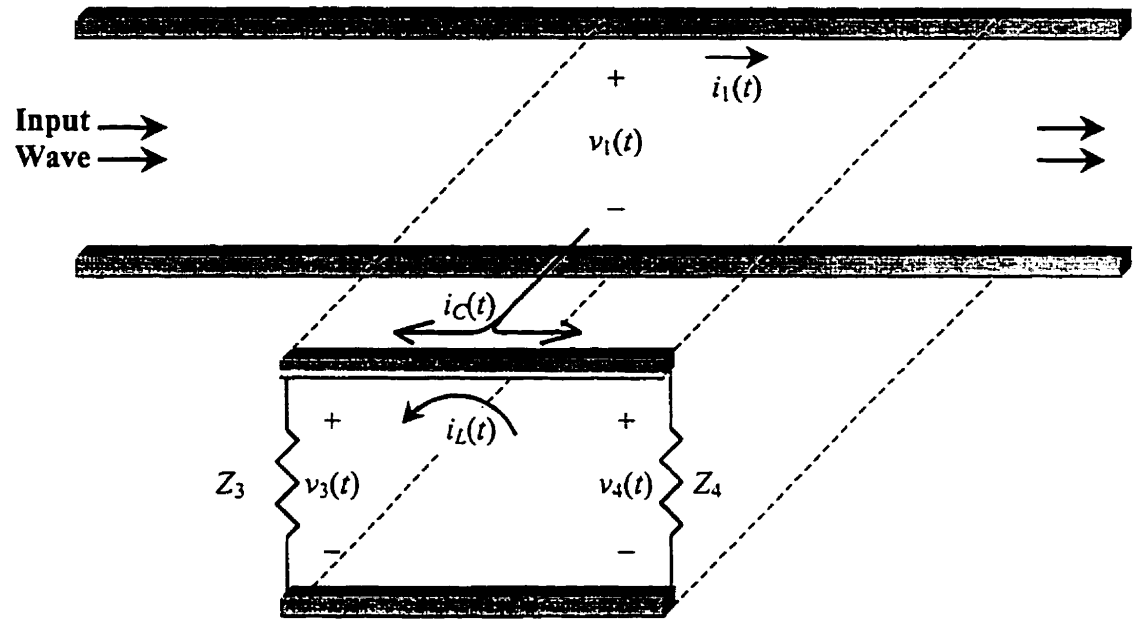

Figure 2-2. Parameters of a coupled elemental length of line.

Under these conditions, the coupled signal becomes directly proportional to the derivative of the input signal, as opposed to the more complex relationship that was presented in Fig. 1-2. As is shown in Fig. 2-2, the capacitive current will be split between Z_3 and Z_4 according to the laws of current division. The inductive voltage will excite an inductive current i_L in a direction dictated by Lenz's Law. The direction of i_L shown in the figure is assuming an increase of i_1 with time.

Given these two contributions of current, the parameters of real interest are the voltages v_3 and v_4 that appear across the terminations of the two coupled ports. If the effects of both inductive and capacitive coupling are combined together then v_4 can be written as

$$v_4 = \frac{Z_4}{Z_3 + Z_4}\left(Z_3 C_m \frac{dv_1}{dt} - L_m \frac{di_1}{dt}\right) \tag{2-23}$$

It can be observed that this voltage will reduce to zero if port #3 is terminated by

$$Z_3 = Z_0 = \frac{L_m}{C_m}\frac{i_1}{v_1} = \frac{L_m}{C_m}\frac{1}{Z_1} \tag{2-24}$$

This shows that if port #3 is properly terminated then the contributions from the inductive and capacitive coupling paths will cancel each other at port #4 causing all the coupled energy to appear at port #3. Indeed, the voltage at port #3 would then be given by

$$v_3 = \frac{Z_3}{Z_3 + Z_4}\left(Z_4 C_m \frac{dv_1}{dt} + L_m \frac{di_1}{dt}\right) \tag{2-25}$$

Backward coupling then is simply the effect of carefully designed constructive and destructive interference at the coupled output ports, through proper terminations of the two closely spaced lines.

It should be noted that in the case of strong coupling, it is no longer possible to analyze the operation of the coupler in terms of just L_m and C_m. This is because the effects of v_2 and i_2 are no longer negligible, and L_{22} and C_{22} must be considered. For this case the analysis [4] becomes more cumbersome, but it is still possible to derive expressions for the terminating impedances which lead to infinite directivity, meaning $v_4 = 0$. In fact, there are a number of different combinations of the terminating impedances of the three output ports that lead to infinite directivity. This is possible as long as certain relations between Z_2, Z_3, and Z_4 are met.

The most common combination of terminating impedances used in coupler designs with symmetric lines is when all the ports are terminated in Z_{11}, or equivalently Z_{22}. This causes v_2 and v_3 to be in phase quadrature over all frequencies, which can be a very useful feature of directional couplers. Also, with these terminating conditions the maximum coupling occurs when the length of the coupled section is an odd multiple of $\lambda/4$.

These terminating conditions can be related to the even and odd mode formulation presented in Section 2.1.2., and specifically to the even and odd mode characteristic

impedances. Using the expressions (2-15) and (2-16) for Z_{0e} and Z_{0o}, it can be shown [8] that, for TEM propagation, i.e., $k_L = k_C$,

$$Z_0 = \sqrt{Z_{0e} Z_{0o}} \tag{2-26}$$

where Z_0 is generally referred to as the coupler impedance. It is interesting to note that physically, Z_0 is actually the characteristic impedance of one line in the presence of the other [9].

2.1.3.2. Coupled-Mode Formulation for Backward Coupling ($k_L = k_C = k$)

With the physical manifestation of backward coupling understood it should now be related to the coupled-mode formulation presented earlier. In this context, backward coupling is defined by the fact that the forward wave a_+ couples only to the backward wave b_-. If the general coupled-mode equations (2-9) and (2-10) are examined further it can be seen that this direction of coupling can only occur if $k_C = k_L = k$. Indeed, for this condition, the coupled-mode equations reduce to

$$(\beta_0 \pm \beta_1) a_\pm = \sqrt{\beta_1 \beta_2}\, k b_\mp \tag{2-27}$$

$$(\beta_0 \pm \beta_2) b_\pm = \sqrt{\beta_1 \beta_2}\, k a_\mp \tag{2-28}$$

and the correspondence between forward waves (+ modes) on one line and backward waves (– modes) on the other line is clear. For this case of equal coupling coefficients, the expression (2-16) for Z_{0o} can be rearranged to show that

$$k = \frac{Z_{0e} - Z_{0o}}{Z_{0e} + Z_{0o}} \tag{2-29}$$

This illustrates an important fact of backward coupling, namely the degree of backward coupling depends solely on the difference between Z_{0e} and Z_{0o}.

Oliver shows in [9] that for a homogeneous medium, such as stripline, the inductive and capacitive coupling coefficients must be equal due to the equality of the even and odd mode phase velocities. This proves that for a coupler present in a homogenous medium the natural coupling direction is backwards.

2.1.4. Forward Coupling

Forward, or co-directional coupling is defined as the case in which the coupled signal propagates in the same direction as the input signal, i.e., the coupled signal would exit port #4 for an input signal at port #1. This is the natural direction of coupling for structures where direct coupling links are present. These structures include waveguide couplers, where the holes in the walls provide the direct coupling links, and branch line couplers, where the two main coupled lines are connected together by two other transmission lines.

To see how these couplers work, the general forward coupling structure shown in Fig. 2-3 will be examined. It will be assumed that all ports are properly terminated, meaning that no reflections occur at the ports, and that an input signal is launched from port #1. When the signal reaches points A, C, and E, part of its energy will be transferred to the other line through the coupling links. Each link will set up two oppositely travelling waves of equal

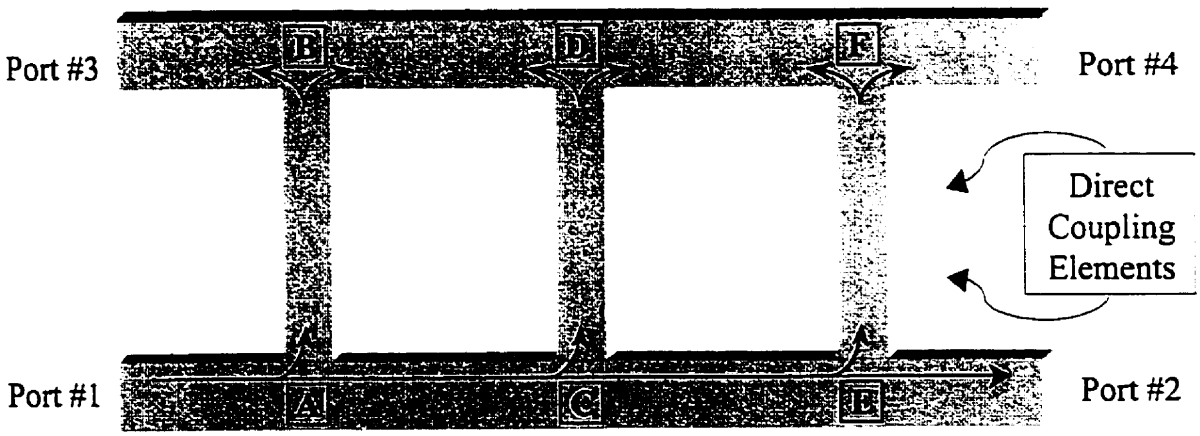

Figure 2-3. General forward coupling structure.

amplitude on the second line. The waves from all the links will reinforce each other at port #4 due to the equal path lengths of ABDF, ACDF, and ACEF. However, the signal at port #3 will be a combination of signals that are out of phase with each other, which leads to destructive interference. Indeed, for couplers operating at a single frequency, complete cancellation is possible if the coupling links are properly spaced. This is how branch line couplers are designed, where the two coupling links are spaced by $\lambda/4$ causing the two coupled signals at port #3 to be 180° out of phase.

On the other hand, for wide-band couplers this design can also be useful. As coupling elements are spaced farther apart it is possible to achieve significant destructive interference over a wider frequency range due to the increase of the phase differences between each of the signals at port #3. As well be shown later, this concept is useful in the design procedure of an RDC.

2.1.4.1. Coupled-Mode Formulation for Forward Coupling ($k_C = -k_L = k$)

Forward coupling can also be achieved with two transmission lines that are not directly coupled through coupling links. This can be seen by rewriting (2-9) and (2-10) for the case $k_C = -k_L = k$

$$(\beta_0 \pm \beta_1)a_\pm = \sqrt{\beta_1\beta_2}\,kb_\pm \tag{2-30}$$

$$(\beta_0 \pm \beta_2)b_\pm = \sqrt{\beta_1\beta_2}\,ka_\pm \tag{2-31}$$

From these equations it can be seen that only forward waves (+ modes) can couple to forward waves and backward waves (– modes) to backward waves.

One way to achieve the condition $k_C = -k_L$ is by adding excess capacitance from each line to ground. This increases the self-capacitance of each line in the absence of the other line. With this extra capacitance it was shown by Oliver in [9] that for symmetric lines,

immersed in a homogeneous dielectric, the phase velocities for the even and odd modes are no longer equal. In fact, the degree of forward coupling increases as this difference in velocities increases. It is also interesting to note that for the necessary amount of excess capacitance that Oliver suggests, the even and odd mode characteristic impedances become equal, resulting in the elimination of any backward coupling.

2.1.4.2. Microstrip Couplers

In a microstrip coupler, the inhomogeneous nature of the dielectric causes the even and odd mode phase velocities to differ. To see why this is so, the electric field patterns for the even and odd modes, as shown in Fig. 2-4, can be examined. From this figure, it can be seen that a small portion of the electric field of the even mode is located in the air, while for the odd mode this portion is larger. Due to the fact that the two modes "see" a different dielectric cross section, the resulting effective dielectric constants are different. This indicates that the phase velocities of the two modes are unequal, which leads to some degree of forward coupling [10]. This means that microstrip couplers have coupling in both the forward and backward directions. With coupling in both directions the directivity of a microstrip coupler can be greatly reduced.

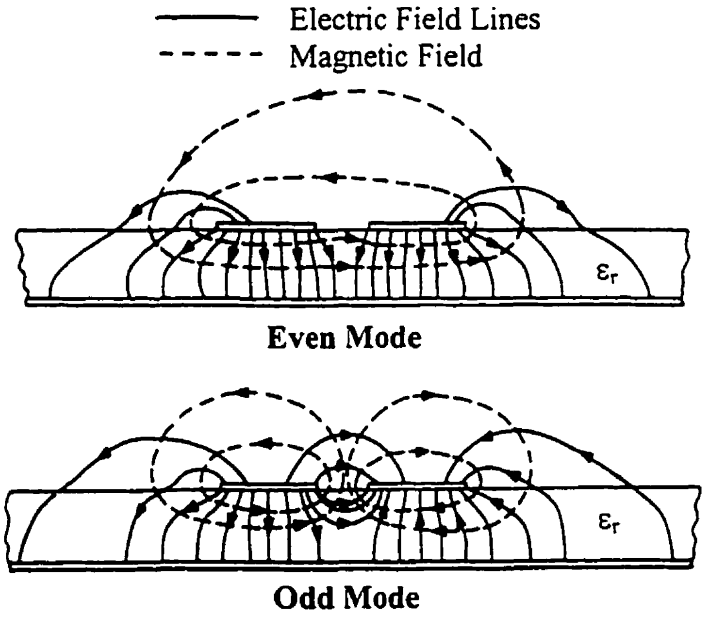

Figure 2-4. Even and odd mode field distributions for coupled microstrip lines.
(From [10], © Artech House, 1996).

Another important property of microstrip couplers is that it is possible to achieve 0 dB (complete) coupling in the forward direction no matter how small the phase velocity difference is. The only requirement is that the length of the coupler be determined by [11]

$$L_{tot} = \frac{\pi}{\beta_e - \beta_o} \tag{2-32}$$

This makes intuitive sense because the length is such that the phase of the even mode has progressed 180° more than the phase of the odd mode. Since the two modes start out 180° out of phase with each other at port #3 then, with this length, they will reinforce each other at port #4, resulting in complete forward coupling.

As an example of this phenomenon, the frequency response of a microstrip edge-to-edge coupler will be presented. The coupler consists of two identical microstrip lines uniformly coupled along its length and has the same layout as the coupler shown in Fig. 1-1. The coupler's design parameters are listed in Table 2-1. The coupler was analyzed using two commercially available full-wave EM simulators as well as a theoretical model of microstrip coupled lines, which will be presented in Chapter 3.

The resulting S-parameters are shown in Fig. 2-5, and from the plot of $|S_{41}|$ it can be seen that full forward coupling (0 dB) is achieved at 4.8 Ghz and 12.3 GHz. It can also be observed that the backward coupling to port #3 ($|S_{31}|$) oscillates about -17 dB.

Table 2-1 Design Parameters for the Microstrip Edge-to-Edge Coupler

w main line width	h dielectric height	s main line spacing	ε_r dielectric constant	L_{tot} total length
0.6 mm	0.635 mm	0.31 mm	9.8	100 mm

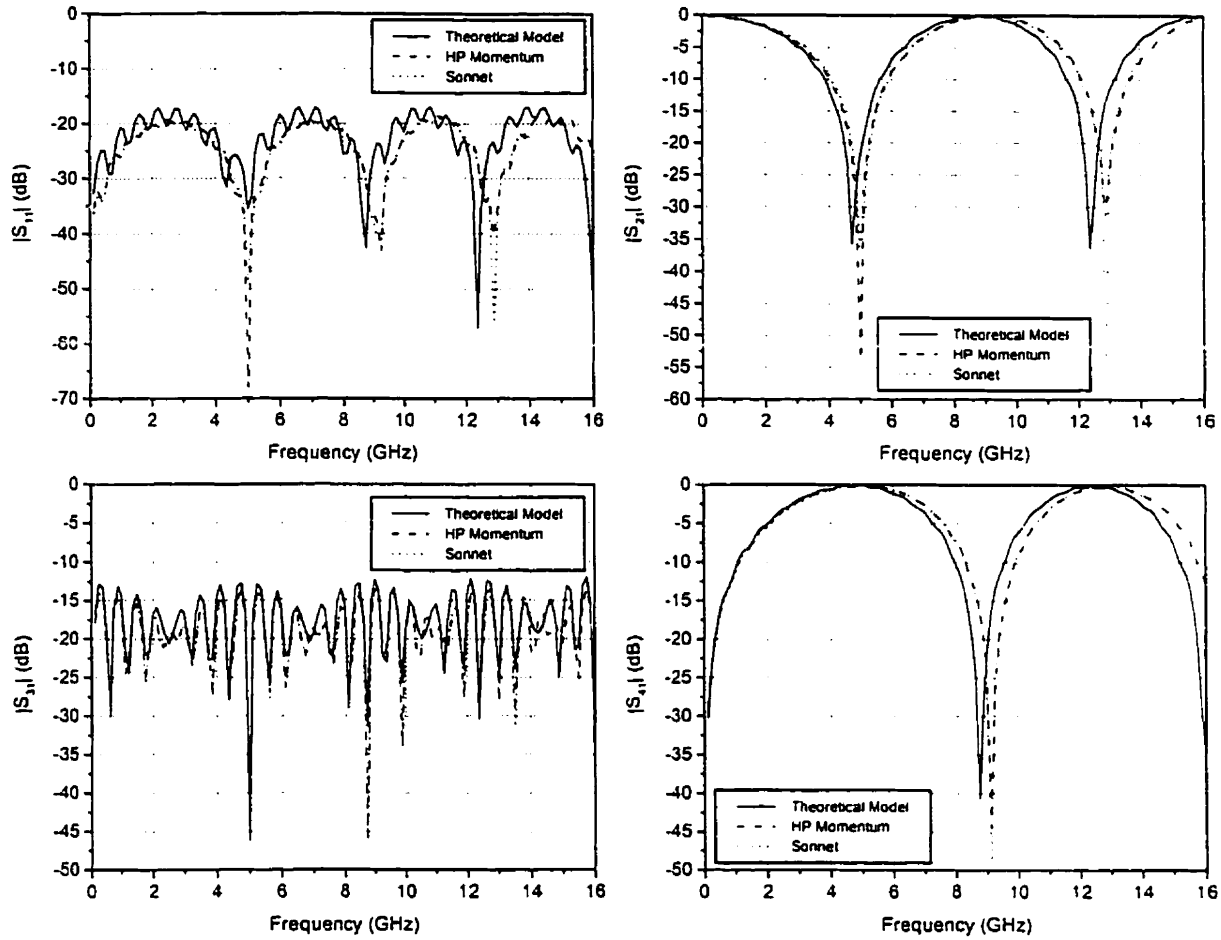

Figure 2-5. S-parameters for a microstrip edge-to-edge coupler.

As (2-32) shows the length, or frequency for a fixed length, at which full forward coupling occurs is a function of the difference between the even and odd mode phase velocities. As this difference is reduced then the necessary length, or frequency, for full forward coupling is increased. Figure 2-6 shows the $|S_{41}|$ characteristic for the microstrip coupler considered above for three different line

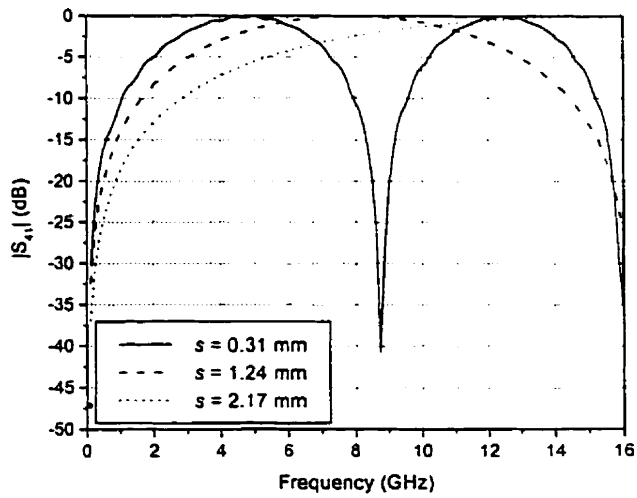

Figure 2-6. Variation of forward coupling with main-line spacing *s*.

spacings. From this figure it is clear that the forward coupling can be reduced over the band of interest if s is increased. For most microstrip directional couplers, the lengths are very short, i.e., $\approx$10 mm – 20 mm, which reduces the effect of this forward coupling. But if longer lengths are required, as is the case for RDCs, then this forward coupling can cause significant problems.

2.2. Conclusions

It has been shown that coupled-mode theory can completely describe the wave behaviour of coupled transmission lines. For symmetric lines, this theory reduces to the even and odd mode theory which can greatly simplify the analysis of the coupler due to the independence of the two modes. It could also be seen that depending on the inductive and capacitive coupling coefficients either forward or backward coupling could be achieved. It has been observed that the strength of the backward EM coupling is determined by the difference between the even and odd mode characteristic impedances. As well, the EM coupling in the forward direction is primarily affected by the difference between the even and odd mode phase velocities. This fact can be seen in microstrip backward couplers where the phase velocities differ and therefore the directivity is reduced due to the unwanted forward coupling. To minimize this, either short couplers can be used or the lines can be spaced farther apart.

Chapter 3

COUPLER ANALYSIS

The RDC designs were analyzed using two methods. First, a theoretical model of the coupler was developed using transmission line theory. Second, the frequency response of a coupler design was determined through the use of two commercially available full-wave EM simulators. The theoretical model was useful due to the short design iterations as compared to the lengthy procedure of full-wave simulation. However, the simulators did provide a reference upon which the theoretical results could be compared and validated. With the frequency response known, it is possible to determine the performance of the coupler response in the time domain. This will be shown to be an invaluable tool in characterizing the performance of an RDC design in a digital environment.

3.1. Theoretical Model

The basic layout, the design parameters and the port definitions of an RDC were shown in Fig. 1-3. The coupler consists of two main transmission lines, which are considered to be good conductors, connected together by a series of resistive lines or strips. In general, these strips are non-uniformly spaced along the length of the coupler but are uniform in their dimensions and sheet resistivity. Table 3-1 outlines the fundamental design parameters of the coupler and the approximate ranges of these parameters used in the research that led to this thesis.

Table 3-1 Design Parameter Definitions for a Resistive Directional Coupler

Symbol	Meaning	Range
w	Width of the main transmission lines.	0.24 mm → 0.62 mm
h	Dielectric thickness, height of conductors above ground. (microstrip)	0.261 mm → 0.635 mm
b	Spacing between ground planes (stripline)	1.27 mm
s	Spacing between the two main transmission lines.	0.1 mm → 6 mm
ε_r	Dielectric constant	2.2 → 12.1
w_r	Width of resistive strips.	10 μm → 3 mm
R_{so}	Surface resistance of resistive strips in Ω/sq.	10 Ω/sq → 10000 Ω/sq
M	Number of resistive strips.	1 → 100
L_1	Length of unit cell.	0.1 mm → 15 mm
L_{tot}	Total length of the coupler.	10 mm → 300 mm

The general procedure for analyzing these couplers using transmission line theory is shown in Fig. 3-1. The first step is to break the coupler up into "unit cells", where each cell contains one resistive strip centered within the cell. This cell can then be analyzed for the even and odd mode excitations separately. As well, with the use of even and odd mode theory the 4-port structure can be transformed into a 2-port device, which greatly simplifies the analysis, as Jenkins and Cullen have shown in [3].

3.1.1. Even Mode Analysis

In the even mode excitation, the voltages on the two main lines are the same. This means that there is a "virtual" open circuit midway between the two lines. Due to this open

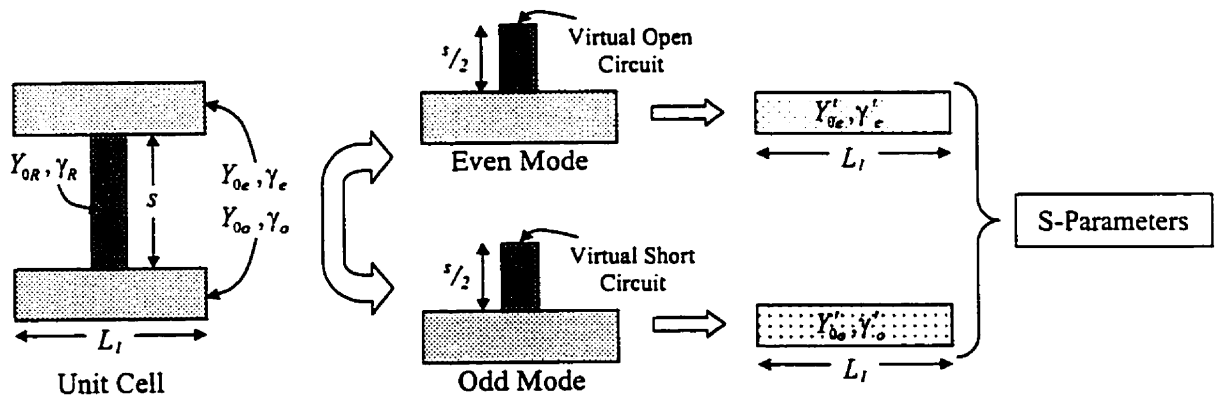

Figure 3-1. Theoretical analysis of a unit cell of the resistive directional coupler.

circuit, a transmission line of length L_1 shunted by an open-circuited resistive stub of length $s/2$ can replace the unit cell. The transmission line has a characteristic admittance Y_{0e} and a propagation constant γ_e, which are determined from an even mode analysis of the two coupled lines without the resistive strips. The resistive stub will load this transmission line according to its input admittance, given by

$$Y_R = Y_{0R} \tanh\left(\gamma_R \frac{s}{2}\right) \tag{3-1}$$

where the resistive strip is characterized by Y_{0R} and γ_R.

Once the line parameters of the transmission line and the resistive stub are known, then the behaviour of this small section of loaded transmission line can be replaced by an equivalent even-mode transmission line. To determine the characteristics of this equivalent line the total ABCD matrix of the loaded line can first be calculated, and is given by

$$ABCD = \begin{bmatrix} \cosh\left(\gamma_e \frac{L_1}{2}\right) & Z_{0e} \sinh\left(\gamma_e \frac{L_1}{2}\right) \\ Y_{0e} \sinh\left(\gamma_e \frac{L_1}{2}\right) & \cosh\left(\gamma_e \frac{L_1}{2}\right) \end{bmatrix} \begin{bmatrix} 1 & 0 \\ Y_{0R} \tanh\left(\gamma_R \frac{s}{2}\right) & 1 \end{bmatrix} \begin{bmatrix} \cosh\left(\gamma_e \frac{L_1}{2}\right) & Z_{0e} \sinh\left(\gamma_e \frac{L_1}{2}\right) \\ Y_{0e} \sinh\left(\gamma_e \frac{L_1}{2}\right) & \cosh\left(\gamma_e \frac{L_1}{2}\right) \end{bmatrix} \tag{3-2}$$

The elements of this matrix are then equated to the elements of the ABCD matrix of the even-mode equivalent line, which is expressed as

$$ABCD' = \begin{bmatrix} \cosh(\gamma'_e L_1) & Z'_{0e} \sinh(\gamma'_e L_1) \\ Y'_{0e} \sinh(\gamma'_e L_1) & \cosh(\gamma'_e L_1) \end{bmatrix} \tag{3-3}$$

The characteristic admittance Y'_{0e} and propagation constant γ'_e are then solved for and are found to be

$$Y'_{0e} = Y_{0e} \sqrt{\frac{2Y_{0e} + Y_{0R} \coth\left(\gamma_e \frac{L_1}{2}\right) \tanh\left(\gamma_R \frac{s}{2}\right)}{2Y_{0e} + Y_{0R} \tanh\left(\gamma_e \frac{L_1}{2}\right) \tanh\left(\gamma_R \frac{s}{2}\right)}} \tag{3-4}$$

$$\gamma_e' = \frac{2}{L_1}\tanh^{-1}\left[\sqrt{\frac{Y_{0R}\tanh\left(\gamma_R\frac{s}{2}\right)+2Y_{0e}\tanh\left(\gamma_e\frac{L_1}{2}\right)}{Y_{0R}\tanh\left(\gamma_R\frac{s}{2}\right)+2Y_{0e}\coth\left(\gamma_e\frac{L_1}{2}\right)}}\right] \tag{3-5}$$

3.1.2. Odd Mode Analysis

A similar procedure can be followed to determine an equivalent transmission line for the unit cell under odd mode excitation. However, in this case, because the line voltages have opposite polarities, there is a "virtual" short circuit midway between the two main lines. This means that the resistive stub loads the line by an admittance given by

$$Y_R = Y_{0R}\coth\left(\gamma_R\frac{s}{2}\right) \tag{3-6}$$

With this loading the parameters of the equivalent odd-mode transmission line are found to be

$$Y_{0o}' = Y_{0o}\sqrt{\frac{2Y_{0o}+Y_{0R}\coth\left(\gamma_o\frac{L_1}{2}\right)\coth\left(\gamma_R\frac{s}{2}\right)}{2Y_{0o}+Y_{0R}\tanh\left(\gamma_o\frac{L_1}{2}\right)\coth\left(\gamma_R\frac{s}{2}\right)}} \tag{3-7}$$

$$\gamma_o' = \frac{2}{L_1}\tanh^{-1}\left[\sqrt{\frac{Y_{0R}\coth\left(\gamma_R\frac{s}{2}\right)+2Y_{0o}\tanh\left(\gamma_o\frac{L_1}{2}\right)}{Y_{0R}\tanh\left(\gamma_R\frac{s}{2}\right)+2Y_{0o}\coth\left(\gamma_o\frac{L_1}{2}\right)}}\right] \tag{3-8}$$

where Y_{0o} and γ_o are the odd mode parameters for the main transmission lines. It should be noted that these equations characterizing the even and odd mode equivalent transmission lines are identical to those found in [3], except the even and odd mode characteristics of the main lines are explicitly stated here.

3.1.3. Calculating the S-Parameters

With each unit cell of the coupler characterized by a length of equivalent transmission line for both the even and odd modes it is possible to calculate the S-parameters of the coupler. The general procedure is outlined in Fig. 3-2. First, the behaviour of the total coupler must be calculated for each mode. This can be done by cascading the *ABCD'* matrices of each cell, for both modes, to obtain $ABCD_e$ and $ABCD_o$.

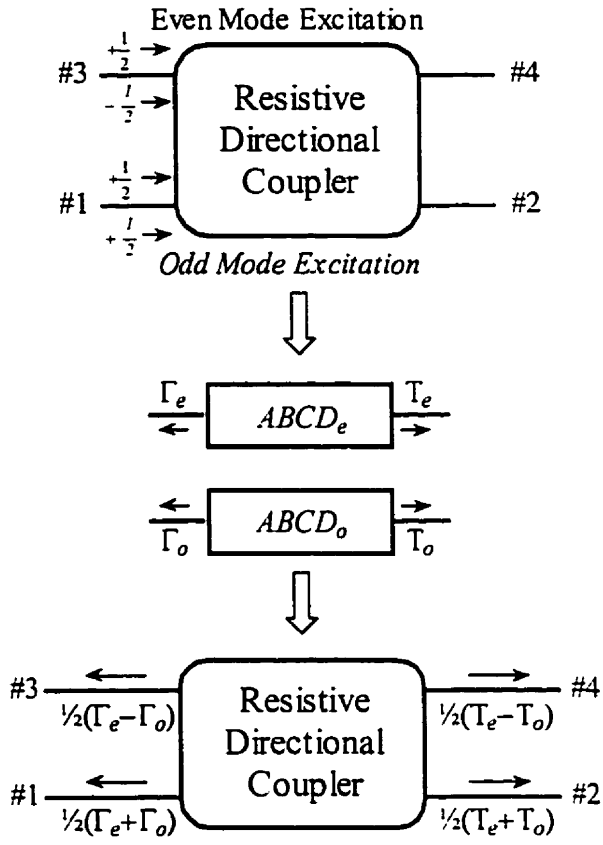

Figure 3-2. Procedure for finding the S-parameters from the even and odd mode ABCD matrices.

For each two-port network that the total ABCD matrices represent, it is possible to calculate the reflection and transmission coefficients from the ABCD parameters. These coefficients are given in terms of the elements of $ABCD_e$ and $ABCD_o$ [12]

$$\Gamma_e = \frac{A_e + B_e/Z_0 - C_e Z_0 - D_e}{A_e + B_e/Z_0 + C_e Z_0 + D_e} \tag{3-9a}$$

$$T_e = \frac{2}{A_e + B_e/Z_0 + C_e Z_0 + D_e} \tag{3-9b}$$

$$\Gamma_o = \frac{A_o + B_o/Z_0 - C_o Z_0 - D_o}{A_o + B_o/Z_0 + C_o Z_0 + D_o} \tag{3-9c}$$

$$T_o = \frac{2}{A_o + B_o/Z_0 + C_o Z_0 + D_o} \tag{3-9d}$$

In these equations, Z_0 represents the reference impedance of system. This reference impedance is the normalizing factor in the calculation of the S-parameters, and is most commonly 50 Ω.

Once these coefficients are known, the results from the analysis of each mode can be combined through superposition. As Fig. 3-2 shows, this results in expressions for the outgoing waves at each port for a unit amplitude input wave at port #1. Thus, the S-parameters can be written as

$$S_{11} = \tfrac{1}{2}(\Gamma_e + \Gamma_o) \tag{3-10a}$$

$$S_{21} = \tfrac{1}{2}(T_e + T_o) \tag{3-10b}$$

$$S_{31} = \tfrac{1}{2}(\Gamma_e - \Gamma_o) \tag{3-10c}$$

$$S_{41} = \tfrac{1}{2}(T_e - T_o) \tag{3-10d}$$

These four equations completely describe the frequency response of a coupler that has transverse symmetry as well as reciprocal properties.

The analysis presented here is more general in nature than the procedure outlined by Jenkins and Cullen [3]. With the use of the transfer matrices, each cell can be individual in its geometry, while Jenkins and Cullen assumed all the cells to be identical. This allows the analysis of couplers that have resistive strips non-uniformly spaced along the coupler. As will be shown later, this can lead to improved performance.

3.1.4. Medium Characterization

The analysis presented above can be used for both microstrip and stripline couplers. This is because the theoretical model requires only the line parameters of the main lines and the resistive strips, and these can be easily found for both environments. The models that were used to calculate these line parameters will now be presented.

3.1.4.1. Microstrip Coupled Lines

Due to the inhomogeneous dielectric, it is a very difficult task to characterize exactly a set of parallel-coupled microstrip lines over a wide range of frequencies. Bryant and Weiss [13] presented one of the first sets of expressions and these were based on a quasi-static assumption that only a TEM mode was propagating. The solutions were determined through the development of a dielectric Green's function, which accounted for the field discontinuity between the dielectric and air interface. With this rigorous analysis then, the results that were presented could be considered to be "exact" as long as the quasi-static assumption can be made. As stated in their paper, this assumption is only valid into the low gigahertz region for typical microstrip dimensions and substrate materials.

Since Bryant and Weiss presented their results, much work has been done to develop a frequency-dependent model for coupled microstrip lines that could maintain its accuracy for a wide variety of coupler parameters over a large range of frequencies. It was shown by Deibele and Bayer in [14] that the analytical expressions presented by Kirschning and Jansen in [15] proved to be the most accurate frequency-dependent model developed thus far. Kirschning and Jansen's empirical equations for Z_{0e}, γ_e, Z_{0o}, and γ_o where derived by matching the approximate results of a rigorous spectral domain hybrid-mode analysis to thousands of numerical data values.

Their procedure contains too many equations to include here but was easily implemented in a Matlab function. The range of validity for their model is

$$0.1 \le w/h \le 10 \quad 0.1 \le s/h \le 10 \quad 1 \le \varepsilon_r \le 18$$

and this is with respect to the frequency of interest as well, which is discussed in terms of a normalized frequency $f_n = f' \cdot h'$ where f' is in GHz and h' is in mm. For the

characteristic impedances, the maximum error is stated to be 2.5% for $f_n = 20$, which is about 31 GHz for a dielectric height h of 0.635 mm. For the couplers examined here, the appropriate parameters fall into a range where the maximum error is reduced to just 1.5%.

3.1.4.2. Coupled Striplines

It is much easier to model two parallel-coupled striplines due to the homogeneous nature of the dielectric. Very early in the development of printed circuit techniques Seymour Cohn presented exact equations for the even and odd mode characteristic impedances for coupled striplines [16]. These equations were derived through the use of conformal mapping and are given as

$$Z_{0e} = \frac{30\pi}{\sqrt{\varepsilon_r}} \frac{K(k_e')}{K(k_e)} \tag{3-11}$$

$$Z_{0o} = \frac{30\pi}{\sqrt{\varepsilon_r}} \frac{K(k_o')}{K(k_o)} \tag{3-12}$$

where K is the complete elliptical integral of the first kind for which closed-form expressions are known. The parameters of the elliptical integrals are given by

$$k_e = \tanh\left(\frac{\pi}{2}\frac{w}{b}\right)\tanh\left(\frac{\pi}{2}\frac{w+s}{b}\right) \tag{3-13a}$$

$$k_e' = \sqrt{1-k_e^2} \tag{3-13b}$$

and

$$k_o = \tanh\left(\frac{\pi}{2}\frac{w}{b}\right)\coth\left(\frac{\pi}{2}\frac{w+s}{b}\right) \tag{3-14a}$$

$$k_o' = \sqrt{1-k_o^2} \tag{3-14b}$$

The propagation constants are the same for both modes for the stripline geometry, and are determined from the speed of light in the medium.

3.1.4.3. Resistive Transmission Lines

The other components of the RDC that need to be modeled are the resistive strips that connect the two main lines. The conventional way to model conductor losses in microstrip and stripline devices is to use the concept of an incremental inductance [17]. This inductance L_i is accompanied by a resistance $R = \omega L_i$, and these two elements are placed in series with the inductance per unit length of the equivalent distributed circuit of the line. However, this method assumes that the line thickness t is much greater than the skin depth δ, i.e., the losses are relatively small. This is not a valid assumption for the high resistance strips that were used for these directional couplers. Instead, the incremental inductance is dropped from the equivalent circuit and the series resistance is given in terms of the surface resistance per square of the strip.

The equivalent circuit, along with a description of its parameters, is shown in Fig. 3-3. From this circuit, the characteristic impedance and the propagation constant can be written as [18]

$$Z_r = R_r - jX_r \tag{3-15}$$

$$\gamma_r = \frac{R}{2R_r} + j\frac{R}{2X_r} \tag{3-16}$$

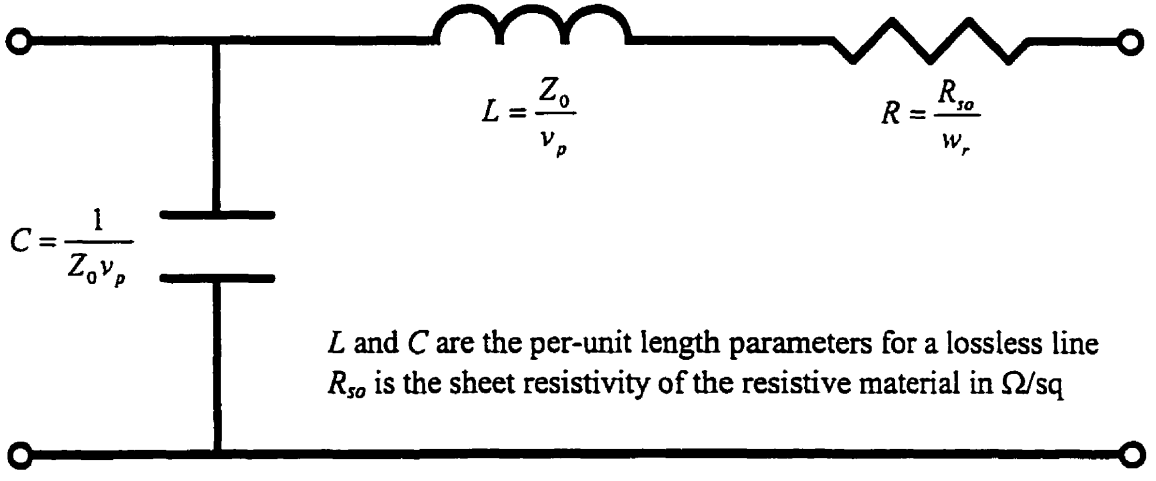

Figure 3-3. Equivalent circuit of the resistive transmission line and its parameters.

with

$$R_r = \sqrt{\frac{\sqrt{\omega L + (\omega^2 L^2 + R^2)}}{2\omega C}} \tag{3-17a}$$

$$X_r = \frac{R}{\sqrt{2\omega C(\omega L + \sqrt{\omega^2 L^2 + R^2})}} \tag{3-17b}$$

These equations are applicable to both the microstrip and stripline cases because only the parameters L and C are medium-dependent. These parameters were determined by calculating the characteristic impedance and the phase velocity within the medium of a single lossless line with the same dimensions as the resistive strip.

3.2. Full-Wave Electromagnetic Simulations

For most of the coupler designs that will be presented, their frequency response was determined through the use of two commercially available "full-wave" EM simulators, HP Momentum and Sonnet. These were used to validate the results obtained from the theoretical model. They are designated as full-wave because they account for every possible coupling mechanism that is present in the structure. This means that the effects of dispersion, discontinuities, surface waves, metalization losses, dielectric losses, and radiation losses [19] are automatically considered. Both these simulators are based on the numerical technique known as the Method of Moments.

3.2.1. The Method of Moments

When an analytical electromagnetic solution is too difficult, or impossible, to achieve then approximate numerical techniques are needed. The Method of Moments is one such technique that is based on transforming an integral equation, which characterizes the

relationship between the electric field and the current present in the structure, into a set of linear equations.

The first step is to approximate the unknown current by a set of N weighted basis, or rooftop expansion functions, similar to the idea of a Fourier series. This can be written as

$$I(z) \approx \sum_{n=1}^{N} I_n F_n(z) \tag{3-18}$$

This approximation can be thought of as splitting the structure into N segments such that the coefficient I_n corresponds to a sample of the actual current $I(z)$ taken from the n^{th} segment. This expression for the current can then be substituted into the integral equation and it can be shown [20] that this replaces the integral equation with the following set of N simultaneous linear equations

$$V_m = \sum_{n=1}^{N} Z_{mn} I_n \tag{3-19}$$

In this equation, V_m represents the complex voltage appearing at the m^{th} segment and Z_{mn} is the mutual impedance between the segments m and n.

Equation (3-19) can be rewritten in matrix form, which leads to the existence of the N by N impedance matrix that completely characterizes the geometry and environment of the structure. The way in which the surrounding medium is characterized for a given structure is different for both simulators. In HP Momentum, the substrate is fully characterized by electric and magnetic Green's functions [21], while Sonnet uses a FFT (Fast Fourier Transform) analysis technique to account for the different layers in a 3-D structure [19]. Once this matrix is determined, and the excitation is set up, meaning the complex voltages are defined for each segment, then it is possible to solve for the only remaining unknown in

(3-19), the current vector. Once the currents are known then the desired parameters, i.e., Y-, Z-, or S- parameters, can be found.

3.2.2. Disadvantages of EM Simulators

The major drawback of these EM simulators is the time it takes to calculate a solution, especially over a wide range of frequencies. In general the analysis time is on the order of N^3 so for electrically large structures this time can be prohibitively long. For the designs analyzed in the course of this research, the average analysis time was on the order of 2-4 days on a Sun Sparc 10.

The time and the complexity of the analysis also depend on the way in which the structure is meshed. For HP Momentum, the cells are individually sized so that small cells are used only where necessary. This method can greatly reduce the total the number of cells, and can make larger structures more feasible to simulate. For Sonnet, the metalization levels are divided up by a set grid space, which means that it takes very long to arrive at a solution for large structures with small elements. For instance, if an RDC has a resistive strip width w_r of 50 μm then the largest possible cell size in the direction along the length of the coupler is also 50 μm. If the coupler's total length is 100 mm then each of the main lines consist of at least 2000 cells. This means that the smallest impedance matrix possible will contain around 4 million elements, which makes the computational time much too long. Due to these different meshing approaches, there are some couplers presented below that could only be simulated with HP Momentum.

3.3. Time-Domain Simulations

The frequency response alone cannot fully describe the performance of a coupler, especially when pulse fidelity is one of the main objectives. The time-domain simulation

indicates how a coupler would respond to an arbitrarily shaped input pulse. The resulting output pulse at each port clearly shows how useful the coupler would be in a digital environment.

With the frequency response already found, it is a simple procedure to simulate the time-domain behaviour of the coupler. This procedure is outlined in the flow chart shown in Fig. 3-4. The output pulse at each port is given by the convolution of the input pulse with the impulse response of the pathway between the input and the output port of interest. The results of this convolution can be more easily calculated in the frequency domain where the convolution integral becomes a multiplication of the two corresponding frequency spectrums. In this case, the frequency spectrum of the impulse response of the pathway between port #1, the input port, and the port of interest, the output port, is the appropriate S-parameter. Therefore, the frequency spectrum of the input pulse should first be found through the use of the Fourier transform, and will be truncated at the highest frequency at which the coupler was simulated. Then, this spectrum is multiplied by each of the four S-parameters, S_{11}, S_{21}, S_{31}, and S_{41}. By taking the real part of the inverse Fourier transform of each of the results the output pulse for each port can be found.

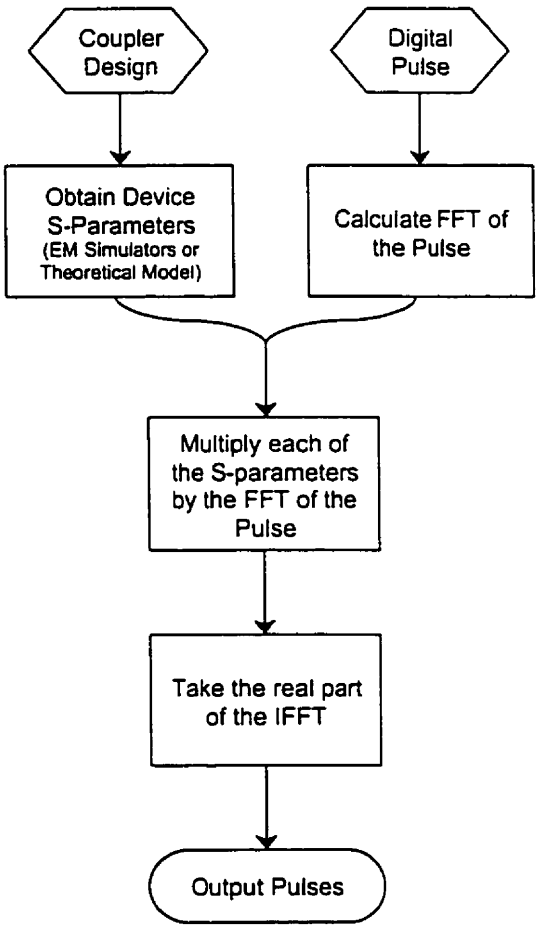

Figure 3-4. Procedure for time-domain simulations.

3.3.1. Input Pulses

In designing an RDC the frequency range of interest must first be determined. The most important criterion is the fact that the main purpose for this coupler design is to provide pulse fidelity in a digital environment. This means that the frequency range of operation should be sufficient to cover the significant portion of the frequency spectrum of the digital pulse being used. However, to reduce the computer simulation time the highest frequency of interest should be minimized.

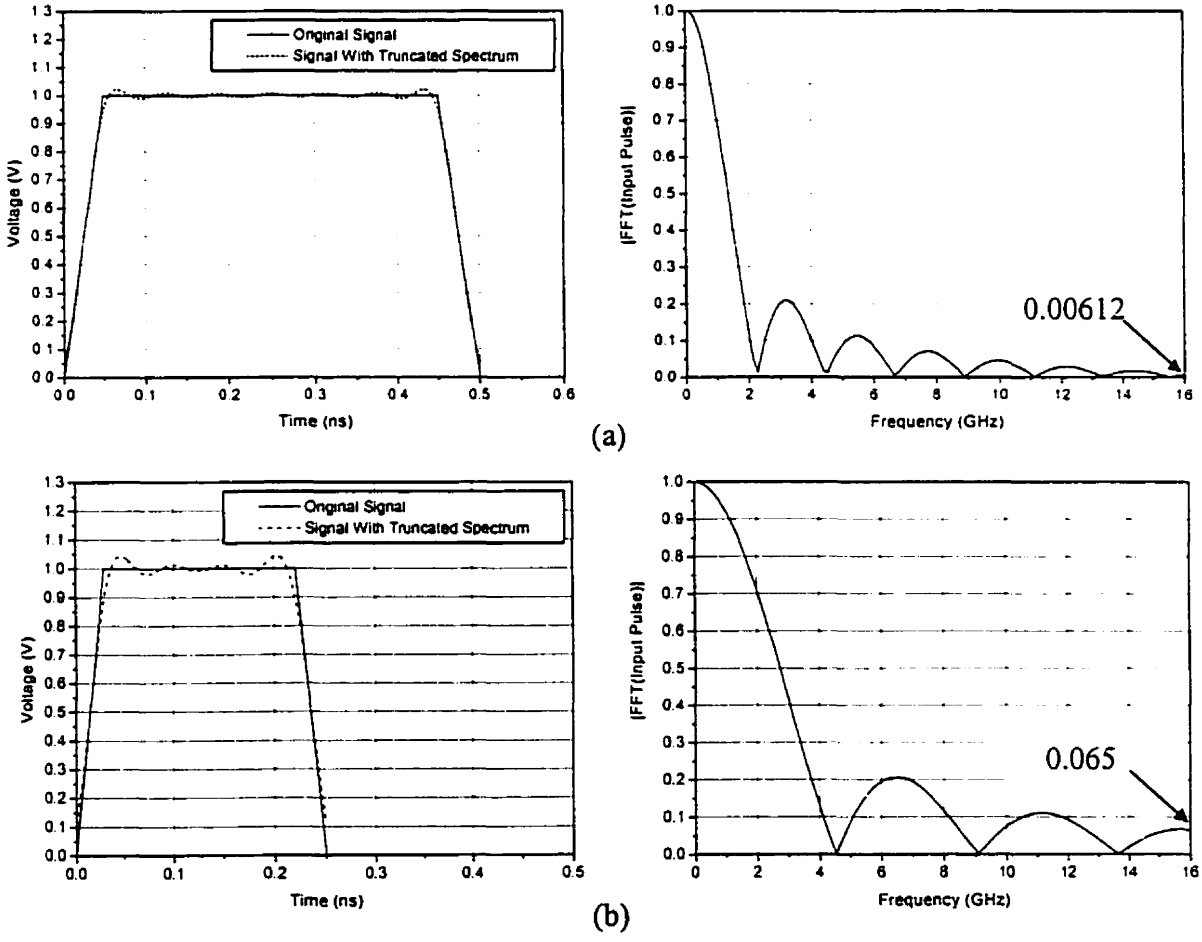

Figure 3-5. Input pulses and their frequency spectrums.
(a) Rise and fall time = 0.05 ns, Total duration = 0.5 ns
(b) Rise and fall time = 0.03 ns, Total duration = 0.25 ns

It is important to first understand what constitutes the significant portion of the frequency spectrum of the pulse. In the design process of the couplers presented here, two rectangular pulses were considered. These pulses, along with their frequency spectra, are shown in Fig. 3-5. It can be seen that for the longer pulse the frequency content above 16 GHz has an amplitude less than 0.7% of the spectrum's maximum value, while for the shorter pulse this amplitude is larger, and is 6.5% of the maximum value. Also shown in Fig. 3-5 are the pulses that have been reconstructed from spectrums that were truncated at 16 GHz. For both pulses, the distortion as a result of this truncation is small enough that they retain their original characteristics. It is clear then, that for both pulses of interest a maximum simulation frequency of 16 GHz will provide sufficient coverage of the pulse's frequency spectrum.

The critical frequency of a pulse is a useful parameter for discussion of the pulse's frequency spectrum. This critical frequency f_0 will be defined as the frequency at which the spectrum first reaches a value of zero. For the longer pulse, $f_0 \cong 2.23$ GHz, while for the shorter pulse, $f_0 \cong 4.55$ GHz. What is interesting about these frequencies, is that over 63% of the total spectral energy is contained below them, i.e., in the range DC $\rightarrow f_0$. This shows the importance of that frequency range in the design of devices that are fed with rectangular pulses.

3.4. Jenkins and Cullen's Resistive Directional Coupler

As an example of the methods of coupler analysis presented here, a coupler presented by Jenkins and Cullen [3] will be examined. This will also give a perspective on the research of RDCs presented here with respect to the only known evidence of related work. The example design that they presented was the beginning point for the work of this thesis, but

their focus was strictly on the frequency-domain behaviour of the RDCs. In this research, the time-domain responses of the RDC designs were also examined. With this added analysis, it will be shown that the time-domain performance of Jenkins' design example is poor and that improvements can be made.

The design parameters of Jenkins' coupler are shown in Table 3-2. The coupler's layout is similar to the general one showed in Fig. 1-3 except that the strips are uniformly spaced along the length of the coupler with a strip-to-strip spacing of 1.4 mm. The coupler's main lines were made from gold, and it was fabricated on a ceramic substrate, which was not specified exactly in their paper. For the analysis here, it will be assumed that the substrate was the common 99.5% alumina substrate that has a loss coefficient of 0.0002.

Table 3-2 Design Parameters of Jenkins' Coupler

w main line width	h dielectric height	s main line spacing	ε_r dielectric constant	w_r resistive strip width	R_{so} sheet resistance	M number of strips	L_{tot} total length
0.62 mm	0.635 mm	1.4 mm	9.8	0.26 mm	50 Ω/sq	22	30.8 mm

The frequency-domain results for this coupler design are shown in Fig. 3-6. In addition to the results from the methods of analysis outlined above, i.e., using the theoretical model and an EM simulator, the experimental results presented by Jenkins and Cullen are also included. All of the simulated results match up quite well with the experimental values except for the higher frequency portion of $|S_{11}|$. Jenkins and Cullen note that this may be due to additional reflections in the experimental set-up due to the transition from the SMA connector to the microstrip line.

This coupler's frequency response is a good example of the general behaviour of an RDC. Both $|S_{11}|$ and $|S_{31}|$ start out at a fairly high DC value and then taper off to lower, more reasonable values at higher frequencies. Also, $|S_{21}|$ and $|S_{41}|$ act very similarly to each other,

in that they stay relatively flat over the first half of the frequency range and then steadily drop for the second half. It should also be noted that the small oscillations, which are observed in the $|S_{11}|$ and $|S_{31}|$ characteristics, correspond to $L_{tot} = \lambda/2$.

The time-domain response of this coupler is shown in Fig. 3-7. The reflection from port #1 is quite large and would cause significant interference with any subsequent incoming pulses. Even though the isolated output pulse at port #3 is somewhat distorted, it almost reaches the same maximum amplitude as the coupled output pulse at port #4. This shows that this coupler has very little "pulse directivity" with the only distinction being the rounded edges of the pulse at port #3. It should also be noted that the output pulses at ports #2 and #4

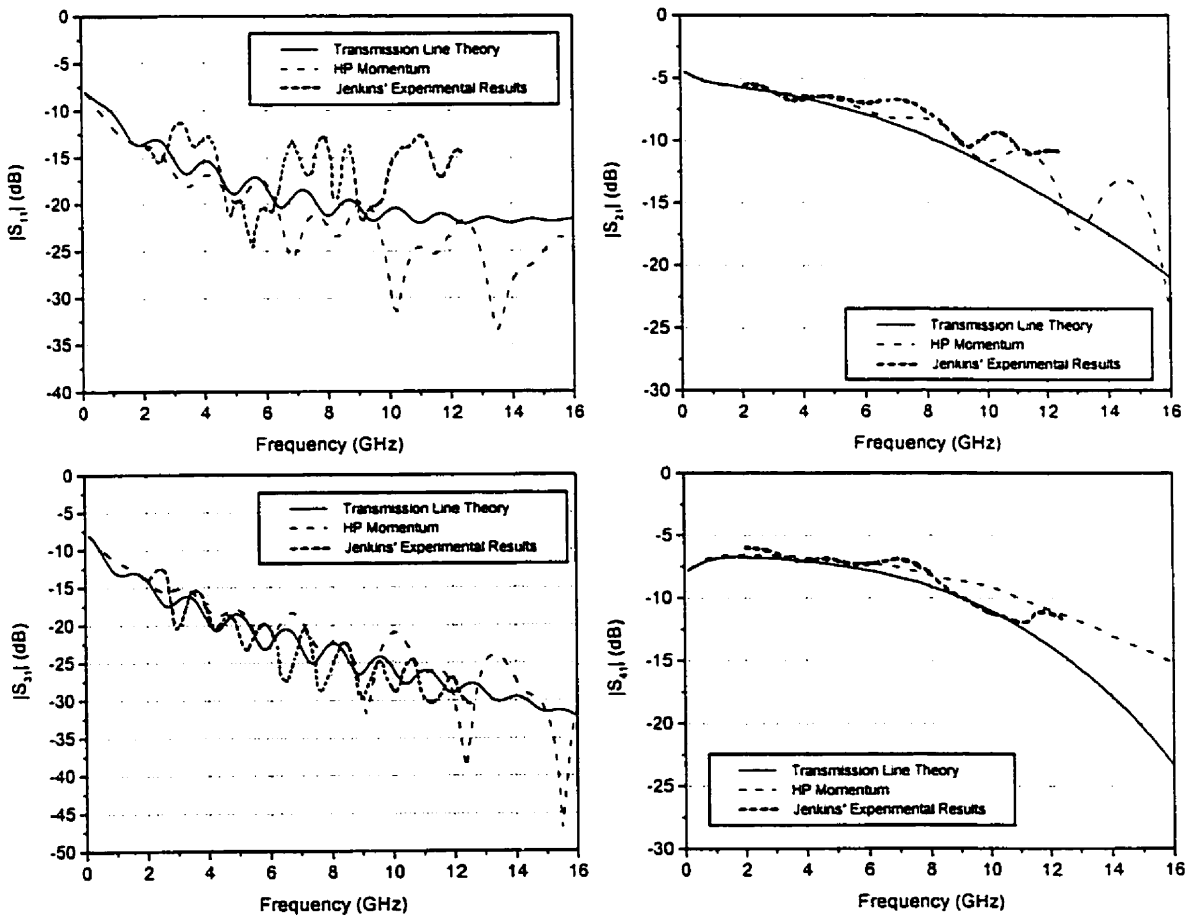

Figure 3-6. S-parameters for Jenkins' resistive directional coupler.

are quite good representations of the input pulse, indicating good pulse fidelity for this coupler.

From the performance of this coupler, the general nature of a resistive directional coupler can be seen. It is clear though, that in order to design a coupler with a reasonable level of directivity and good pulse fidelity more research into the behaviour of this branch of directional couplers is needed.

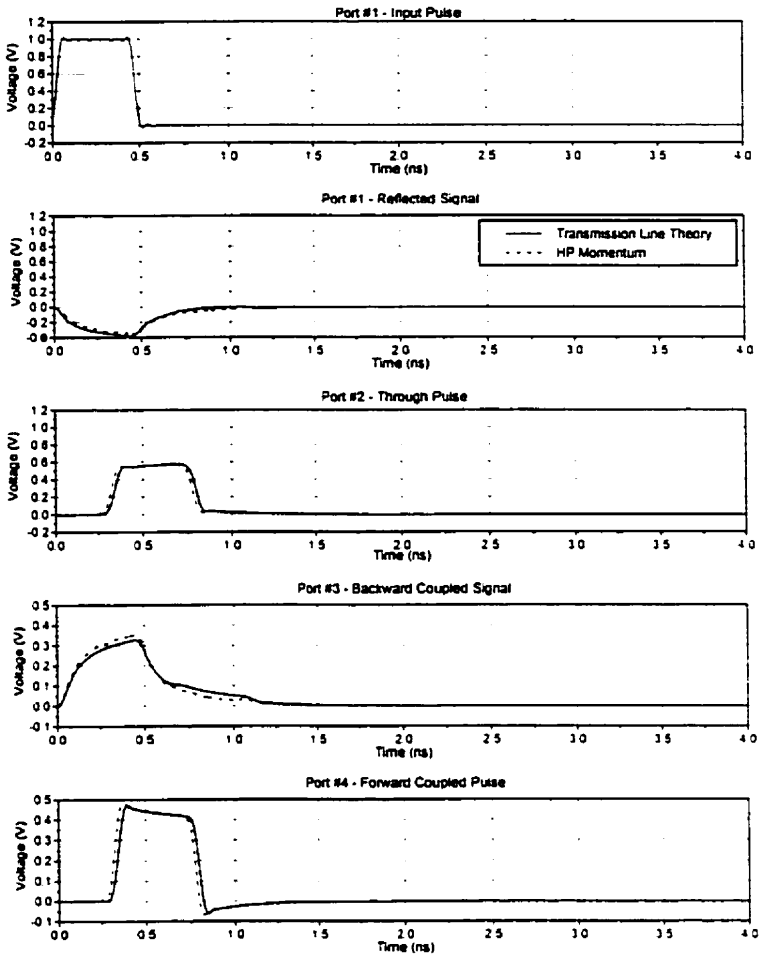

Figure 3-7. Time-domain response of Jenkins' resistive directional coupler.

Chapter 4

RESISTIVE DIRECTIONAL COUPLER DESIGN

The main objectives for an RDC design are pulse fidelity, directivity, level of coupling, and total allowable losses. These objectives will be introduced and in particular, the method of quantifying pulse fidelity, and the concept of pulse directivity will be discussed in detail. With these goals in mind, specific design guidelines will be presented that outline the effects of various parameters on the coupler's performance. These guidelines will be used to develop a procedure for synthesizing RDC designs to meet a given set of specifications. This procedure will then be applied to a variety of coupler designs for both stripline and microstrip environments.

4.1. Design Objectives

4.1.1. Pulse Fidelity

True pulse fidelity results in perfect replication of an input pulse to the desired destinations within a device. In a directional coupler there are two destinations of interest, namely the through port (port #2) and the coupled output port (port #4). In reality it is impossible to achieve perfect replicas, so the goal becomes achieving pulses that will reliably carry on the information to other devices within the system.

This notion of pulse fidelity is a useful one because it eliminates the need for any post-processing of the coupled signal. As was shown in the Introduction, for most directional couplers the coupled pulse is proportional to the derivative of the input pulse. This results in two pulses of opposite polarity that indicate when the edges of the input pulse occur in time. The original pulse can then be reconstructed from this information, but this adds a certain amount of complexity to the circuit.

4.1.1.1. Scale of Pulse Fidelity

In order to be able to specify the required level of pulse fidelity, it is important to be able to quantitatively characterize a coupler's fidelity performance. To achieve this, a "scale of pulse fidelity" will be presented here, with the intention that it provide a good indication of how accurately the input pulse is replicated at the three output ports.

For each output signal, the degree to which it represents the input pulse can be determined by a correlation coefficient. This coefficient can be calculated for each instant in time from [22]

$$\rho(\tau) = \frac{r(\tau)}{\sqrt{\int_{-\infty}^{\infty} s_1^2(t)dt \int_{-\infty}^{\infty} s_2^2(t)dt}} \tag{4-1}$$

where $r(\tau)$ is the cross-correlation of the two signals $s_1(t)$ and $s_2(t)$, and $\rho(\tau)$ always lies between 0 and 1. Once $\rho(\tau)$ is determined over the appropriate time interval, its maximum value is used to represent the fidelity of the output pulse. It has been observed that when the maximum correlation coefficient falls below 0.6 the output pulse that it corresponds to is significantly distorted and spread out in time. For this reason, the "scale of pulse fidelity" will be a re-scaled version of the maximum correlation coefficients, with 0.6 being mapped to zero. This will allow greater resolution in the scale so that a clearer picture of what the output pulse looks like can be obtained.

To give the reader a feel for this scale, a number of pulses, along with its scale value, which will be termed the fidelity value, are presented in Fig. 4-1. All of these output signals were compared to the pulse shown in Fig. 3-5(a), which had a rise and fall time of 0.05 ns and a total duration of 0.5 ns. In the graphs shown, only the time scale has been included, because the correlation coefficients are normalized by the signal amplitudes.

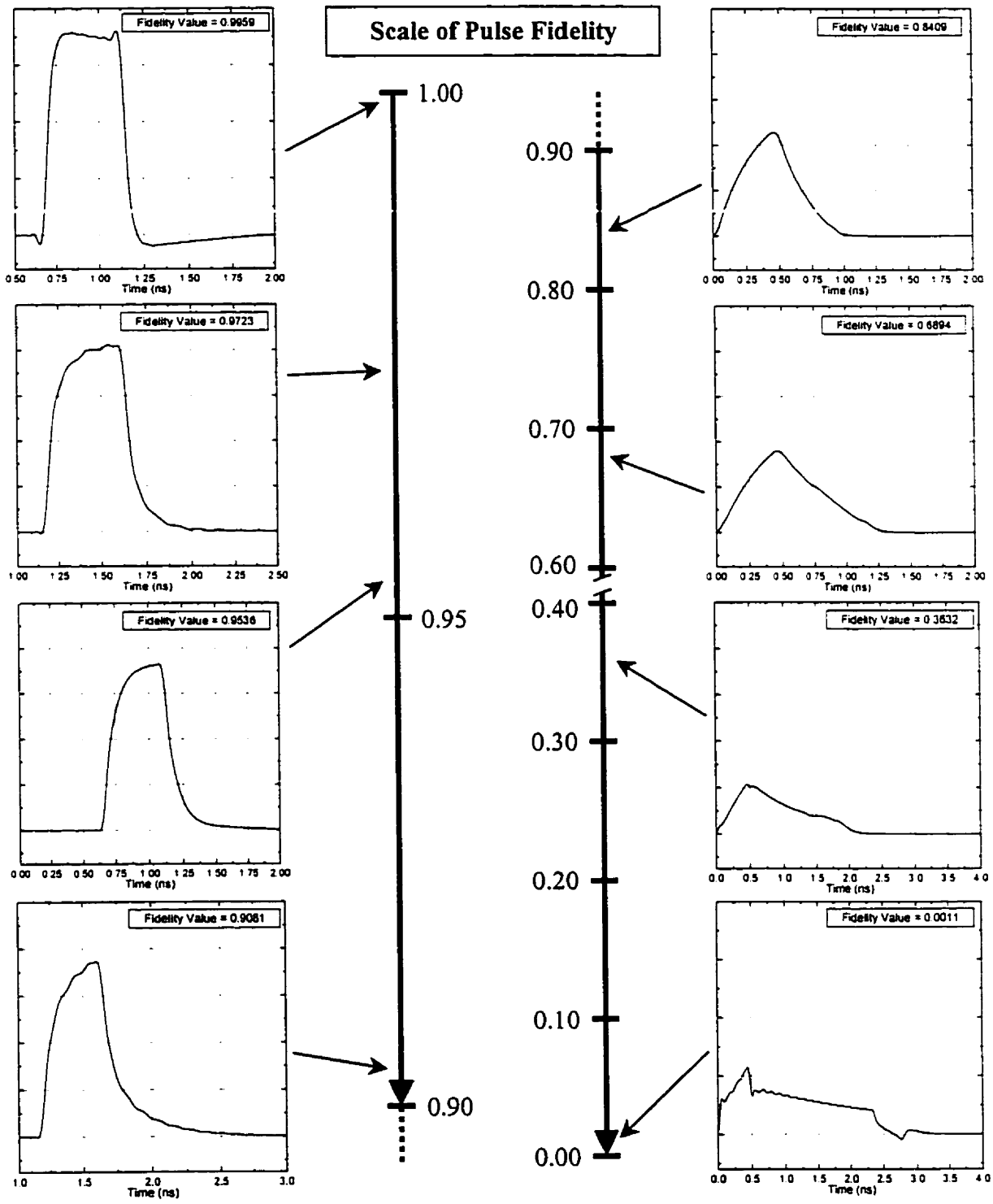

Figure 4-1. Example pulses along the scale of pulse fidelity.

In fact, the fidelity value is really a measure of how much the output pulse has been spread out in time. For example, the pulse with the lowest fidelity value, 0.0011, shown in Fig. 4-1 still maintains some resemblance to the input pulse. However, its duration is five times longer than that of the input pulse, resulting in its low fidelity value. In characterizing the fidelity performance of an RDC, the value attributed to this output signal would be accurate in its implication to the designer. This is because, the higher level of signal distortion leads to a signal which is more spread out in time.

Although the degree of pulse fidelity is a choice of the designer, a general guideline that the fidelity value should be greater than 0.97 to achieve good pulse replication can be inferred from Fig. 4-1. For the isolated pulse, sufficient distortion occurs for fidelity values below 0.4.

4.1.2. Directivity

Another important objective of an RDC is to achieve a certain level of signal directivity between the two coupled ports. Most commonly, the directivity for a coupler is defined by the difference between the coupling to the two ports of the coupled line and is usually specified for a certain bandwidth. However, this definition does not shed any light on the performance of the RDC. This is because the conventional directivity is essentially a frequency parameter, while the domain of most interest in the RDC is the time domain.

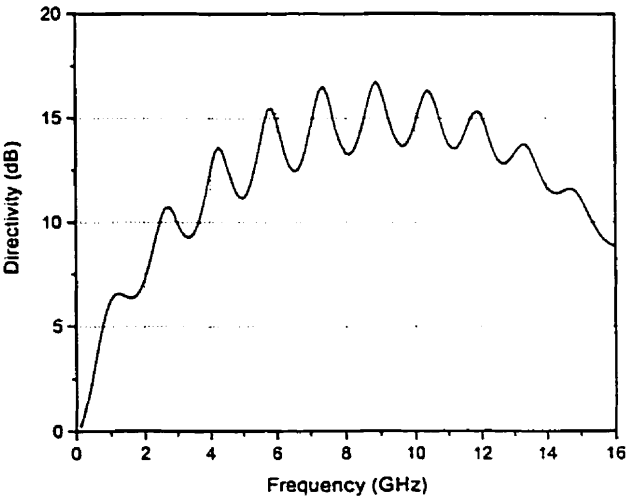

Figure 4-2. Conventional definition of directivity for Jenkins' coupler.

For example, the conventional directivity, defined as $20\log_{10}|S_{41}/S_{31}|$, for Jenkins' coupler discussed in Chapter 3 is shown in Fig. 4-2 as a function of frequency. Over the range of 6 GHz – 12 GHz it could be said that the coupler maintains a directivity of 14 dB ± 1dB. Although that is not a very good directivity, it still does not convey how poor the directivity of the coupled pulses is in the time domain, as was shown in Fig. 3-7.

4.1.2.1. Pulse Directivity

As an alternative definition to the standard one, the directivity will be determined from the energies contained within the two coupled signals. This eliminates the need to specify a bandwidth for the directivity and gives a clearer physical insight into the operation of the RDC.

To calculate the energy of a signal, the signal's power must first be determined. To do this a 50 Ω termination for all the ports is assumed. With this assumption, the instantaneous power of the signal at port n can be written as

$$P_n(t) = \frac{v_n^2(t)}{50} \tag{4-2}$$

Since energy is related to power through an integral over a certain time interval, the signal's energy can be written as

$$E_n = \int_0^{t_0} P_n(t)dt = \frac{1}{50}\int_0^{t_0} v_n^2(t)dt \tag{4-3}$$

where after the time t_0 the value of the signal remains zero.

Once the signal energies are found for both the coupled ports, the energy directivity, in decibels, can be defined as

$$D_E = 10\log_{10}\left(\frac{E_4}{E_3}\right) \tag{4-4}$$

and this will be the definition used to characterize the coupler designs presented in this thesis. However, this definition produces much lower directivities than are normally associated with good directional couplers, e.g. 15 dB → 40 dB. Instead, energy directivities on the order 4 dB → 10 dB will represent couplers with good directional performance.

4.1.3. Coupling Level

The coupling level is one of the most important specifications of a directional coupler. In a coupler where a pulse is the signal of interest, the DC coupling value determines the coupling level. This is because the level of the flat top of the coupled pulse is only affected by the coupling at DC.

To determine an expression for the coupling level in terms of the coupler parameters, the coupler must be analyzed at DC. To this end, an RDC can be characterized at DC by a simple resistor network, like the one shown in Fig. 4-3. In this figure, R_{tot} is the total resistance between the two main lines and is calculated from the parallel connection of all of the resistive strips. In terms of the coupler's geometrical parameters this total resistance can be written as

$$R_{tot} = \frac{1}{M}\frac{s \cdot R_{so}}{w_r} \tag{4-5}$$

where it has been assumed that all the strips are the same.

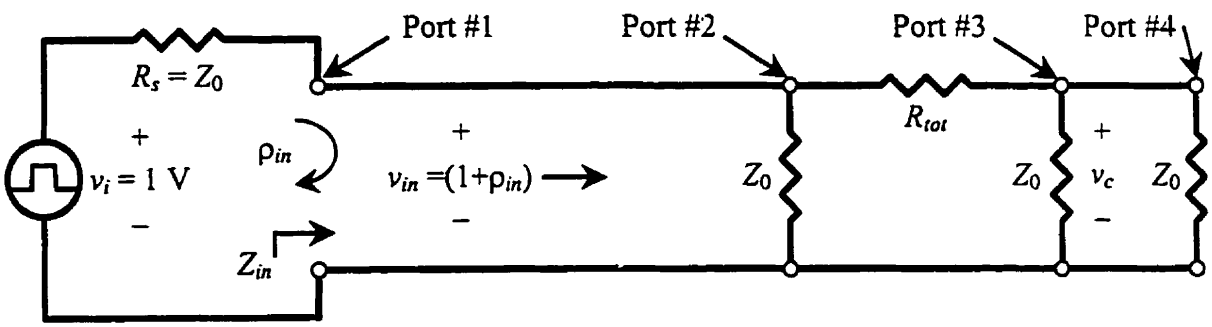

Figure 4-3. DC equivalent circuit of a resistive directional coupler.

The coupling level is determined by analyzing the circuit shown in Fig. 4-2 and solving for the voltage v_c. The reflection coefficient at port #1 can be determined from the DC input impedance of the coupler, and is thus written as

$$\rho_{in} = \frac{Z_{in} - Z_0}{Z_{in} + Z_0} = \frac{1}{2}\left(\frac{-Z_0}{Z_0 + R_{tot}}\right) \tag{4-6}$$

It can be noted that to minimize the reflection of the input pulse, R_{tot} should be maximized. Once ρ_{in} is found then v_c follows from voltage division, and since the input voltage is 1 V, the coupling in dB can be written as

$$C_{dB} = 20\log_{10}[v_c] = 20\log_{10}\left[\frac{1}{2}\left(\frac{Z_0}{Z_0 + R_{tot}}\right)\right] \tag{4-7}$$

This equation can be used to determine the necessary R_{tot} for a given coupling level. Once this is set, the necessary values of the geometrical parameters can be determined from (4-5).

4.1.4. Losses

Although there are considerable losses associated with the use of an RDC, one may want to specify the maximum possible loss for a coupler design. This means that the value of the total loss should be monitored throughout the design procedure. To do this, the energy that appears at each port should first be found so that the total output energy is known. To determine the percentage of the input energy that is lost, the total output energy is subtracted from the energy contained within the input pulse. Although this may not be an exact analysis by considering the individual loss mechanisms of the coupler, it does provide a good sense of how the design performs.

As will be seen later, there is generally a tradeoff between lower losses, and good directivity and fidelity performance. Also, as Jenkins and Cullen showed in [3, see Fig. 3], the losses increase as the coupling becomes stronger. In fact, for an RDC that has 3 dB

coupling, meaning in the lossless case the input power would be shared between the through port and the coupled port, the losses rise to 3 dB. This means that the actual coupling to port #4 is only 6 dB.

4.2. Design Guidelines

In order to understand how to design an RDC a study of the effects of the individual design parameters was done. For a general stripline coupler design, each parameter was swept over a reasonable range and for each value the coupler response was simulated using the theoretical model. Calculating the distortion of the signals at ports #2, #3 and #4, the directivity, and the distribution of energy throughout the coupler fully characterized the coupler's performance. The fact that the results over wide parameter ranges were so quickly obtained signifies how useful the model was, as compared to the full-wave EM simulators. The results of this study for this design proved, with further research, to be indicative of how these parameters affected the coupler performance in general. For this reason, these results will now be presented for the parameters that made a noticeable difference in the coupler performance as they were changed.

4.2.1. Design Parameter Effects

The parameters M, s, w_r, and L_{tot} were found to have a significant effect on the coupler performance as their values were changed. For each test of the parameters, the total resistance R_{tot} was kept constant as the parameter values were swept. This allowed the performance of each design to be properly compared to the designs generated by other values of the same parameter. To achieve this constant R_{tot}, R_{so} was changed for the studies of the parameters M, s, and w_r.

The coupler design, upon which these parameter tests were based, is given by the design parameters shown in Table 4-1. The coupler was implemented in a stripline environment so that the effects of the inhomogenous dielectric did not need to be considered. It should also be noted that the dielectric and conductor losses were neglected in this analysis due to the fact that these would be considerably smaller than the losses of the resistive strips.

Table 4-1 Design Parameters of the Stripline Coupler Used for the Parameter Tests

w main line width	b ground plane spacing	s main line spacing	ε_r dielectric constant	w_r resistive strip width	R_{so} sheet resistance	M number of strips	L_{tot} total length
0.24 mm	1.27 mm	0.8 mm	9.8	0.05 mm	50 Ω/sq	20	60 mm

4.2.1.1. Effects on Pulse Fidelity

Figure 4-4 shows the effects of M, s, w_r, and L_{tot} on the coupler's pulse fidelity. It can be seen from Fig. 4-4(a) and 4-4(b) that as M and s increase there is initially a large drop in the fidelity value of the pulse at port #3. During this initial period, the fidelity values of the through pulse and the coupled pulse stay relatively constant. This means that it is possible to achieve good pulse replication at ports #2 and #4 and good pulse distortion at port #3. After this period, as M and s are increased further the fidelity of the pulses at port #2 and #4 drops below acceptable values, i.e., <0.97. It should be noted that the increase of s has a more profound effect on these pulses than does the increase of M.

In the frequency domain, these effects of increasing M and s were observed by the fact that $|S_{21}|$ and $|S_{41}|$ dropped off more rapidly with frequency. This shows that as s becomes electrically larger its attenuating factor has a significant effect over a wider range of frequencies. This causes the higher frequency portions of the pulse to be diminished leading to rounded pulses and eventually total loss of their rectangular shape.

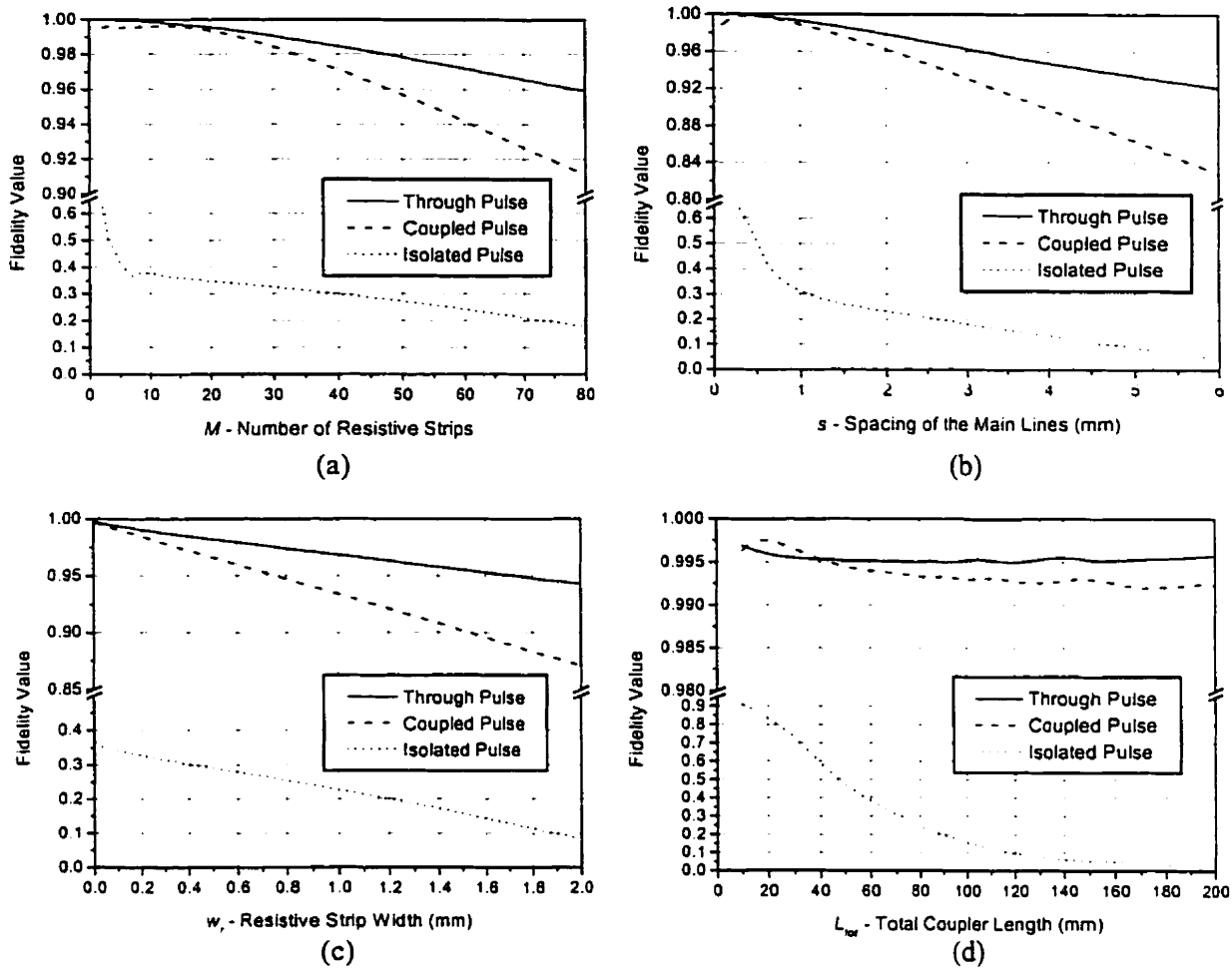

Figure 4-4. Effects of M, s, w_r, and L_{tot} on the pulse fidelity of the coupler.

However, if an attempt is made to improve the fidelity by using small s values the close spacing of the main lines will lead to large EM coupling at port #3. Table 4-2 shows the EM coupling values for a variety of line spacings in both stripline and microstrip environments. These values were determined from (2-29) which expresses the coupling coefficient in terms of the even and odd mode impedances of the coupler. It can be seen that if $|S_{31}|$ is to be kept below 40 dB to create a certain level of directivity for a weak-coupling stripline RDC then s must be greater than 1.5 mm. This large s may then reduce the fidelity of the coupler, highlighting the trade-off between fidelity and directivity that is present in the design of an RDC.

Table 4-2 Approximate Coupling Values for Various Edge-to-Edge Couplers

	Stripline (w = 0.24 mm, b = 1.27 mm, ε_r = 9.8)				**Microstrip** (w = 0.62 mm, h = 0.635 mm, ε_r = 9.8)			
	Spacing between coupled lines (s)							
	0.1 mm	0.6 mm	1.2 mm	1.5 mm	0.1 mm	0.8 mm	1.5 mm	2 mm
Coupling	-8 dB	-20 dB	-33 dB	-39 dB	-8 dB	-19 dB	-25 dB	-34 dB

The effects on the pulse fidelity of the two parameters w_r and L_{tot} are shown in Fig. 4-4(c) and 4-4(d), respectively. To achieve good pulse fidelity for ports #2 and #4, w_r should be kept as small as possible. However, manufacturing tolerances may limit the extent of which w_r can be minimized. It is interesting to note, that the total coupler length does not degrade the pulses at ports #2 and #4 much at all. This allows the length to be increased so that the pulse seen at port #3 becomes more distorted. However, in today's microwave circuits real estate is at a premium and therefore the requirement of long lines, on the order of 50 mm – 200 mm, may not be able to be met. Indeed, the need for long lines is one of the major disadvantages of the RDC.

4.2.1.2. The Effects on Directivity

For an RDC the most difficult objective to achieve is directivity. This is because at DC the coupler looks like a simple resistor network and there is no distinction between ports #3 and #4, as can be observed from Fig. 4-3. The only way to produce a directive effect is by distorting the pulse at port #3 while maintaining good input pulse replication at port #4.

To see how this distortion comes about, it is important to understand the make-up of the signal at port #3. As was discussed in Chapter 2, for forward couplers with direct connections the backward coupled signal is a result of the addition of many different signals, one for each of the resistive strips, as well as the contribution from EM coupling. The signals contributed from the strips have each traveled different path lengths due to the placement of the strips. Therefore, it should be expected that a coupler with many resistive

strips that are spaced far apart from each other would result in many signals with large phase differences, which would increase the distortion of the signal at port #3 and thus increase the directivity.

The characteristics of the effects of the design parameters on the coupler directivity are shown in Fig. 4-5. In Fig. 4-5(a), it can be observed that above a certain value for M there is not much improvement in the directivity. This is a surprising result since it was thought that the increased distortion of the signal at port #3 due to the addition of more strips would cause the directivity to increase as well. However, as more strips are added the distortion of the pulse at port #4 increases as well, resulting in a directivity characteristic that levels off.

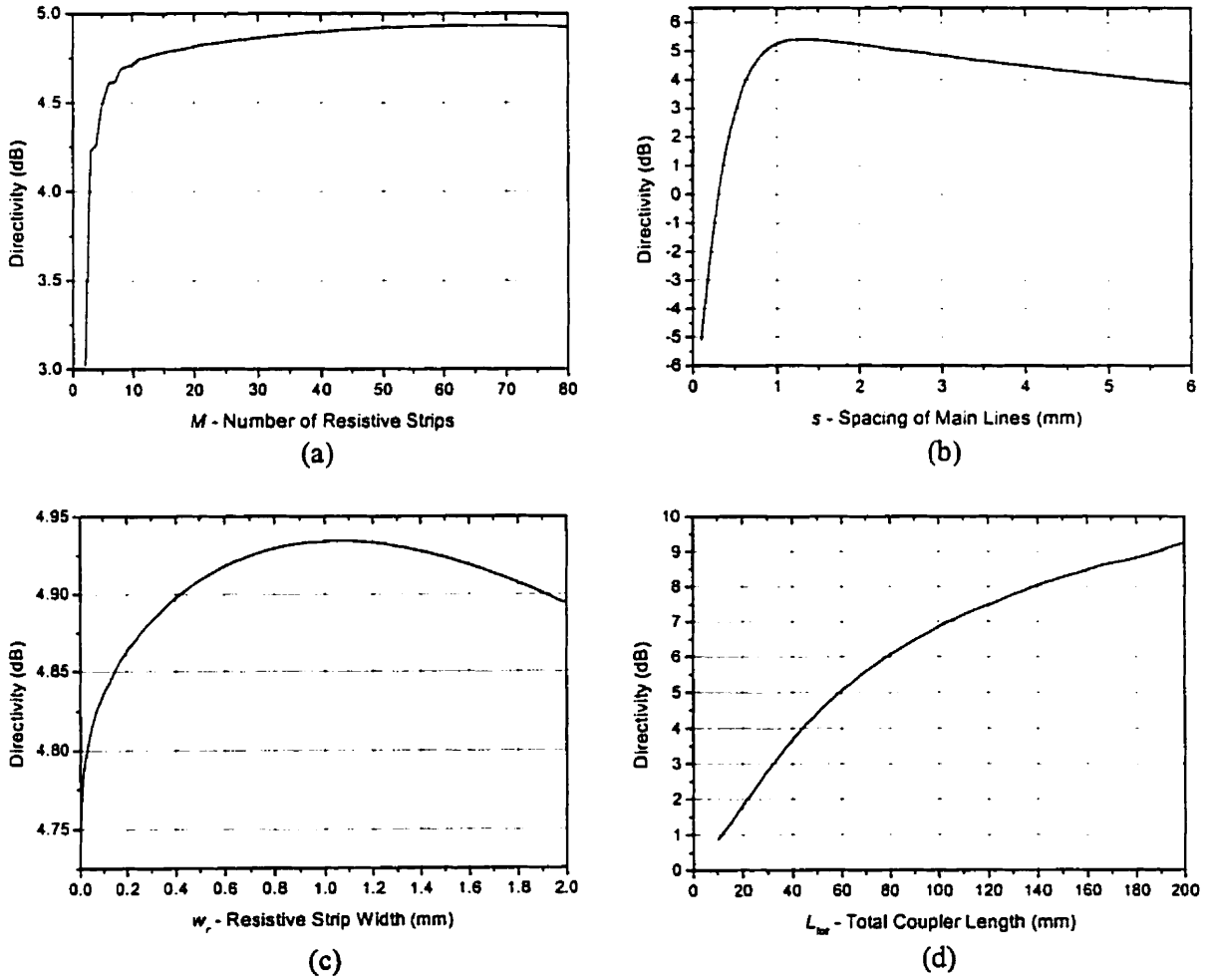

Figure 4-5. Effects of M, s, w_r, and L_{tot} on the directivity of the coupler.

A similar profile for the effect of s on the directivity can be see in Fig. 4-5(b). In this case, the directivity reaches a maximum value and then drops slightly as s is increased further. The negative values of the directivity observed for small values of s, indicate the strength of the EM coupling is diverting most of the coupled energy to port #3. The effects on the directivity of M and s indicate that there is most likely a combination of these two parameters that will maximize the coupler directivity. Indeed, as will be apparent later in the design procedure of the RDC designs, this is the case.

From Fig. 4-5(c), the effect of w_r on the directivity can be seen. Although there is a peak that is reached, the changes in the directivity are very small. This indicates that as w_r increases, both of the coupled signals are affected in the same way resulting in a nearly constant directivity profile.

On the other hand, as can be seen in Fig. 4-5(d), the total length of the coupler has the greatest effect on the directivity observed thus far. In fact, it appears that the directivity would continue to improve if the length was increased further.

As was mentioned above, longer couplers can lead to improved directivity due to the increase of phase differences between the signals that appear at port #3. Another perspective of why long couplers lead to improved directivity at port #3 can be obtained by examining the frequency-domain response of the coupler. It has been mentioned in Section 3.3.1 that when the signals of interest are rectangular pulses the most significant frequency range is from DC to f_0. This means that within this range $|S_{31}|$ should be a low as possible, while $|S_{41}|$ should ideally be flat.

The DC values of both of these S-parameters are equal according to the desired level of coupling, as was shown in Section 4.1.3. Therefore, $|S_{31}|$ should drop rapidly, with respect to frequency, from this DC value. As was mentioned in Section 3.4, the oscillations that are

present in the $|S_{31}|$ characteristic are a function of the total coupler length. Therefore, as the length of the coupler increases the resonant frequency decreases and $|S_{31}|$ changes more rapidly.

It has been observed that generally $|S_{31}|$ will drop to an average value that closely corresponds to the strength of the EM coupling present between the two main lines. This shows that the contributions from the resistive strips to the isolated port signal tend to cancel each other out, or at least reduce their combined effect, at higher frequencies.

4.2.1.3. Effects on Dissipated Energy

In Fig. 4-6, the curves of most interest are the ones that represent the dissipated energy of the coupler. For each of the parameters, the amount of lost energy increases as the

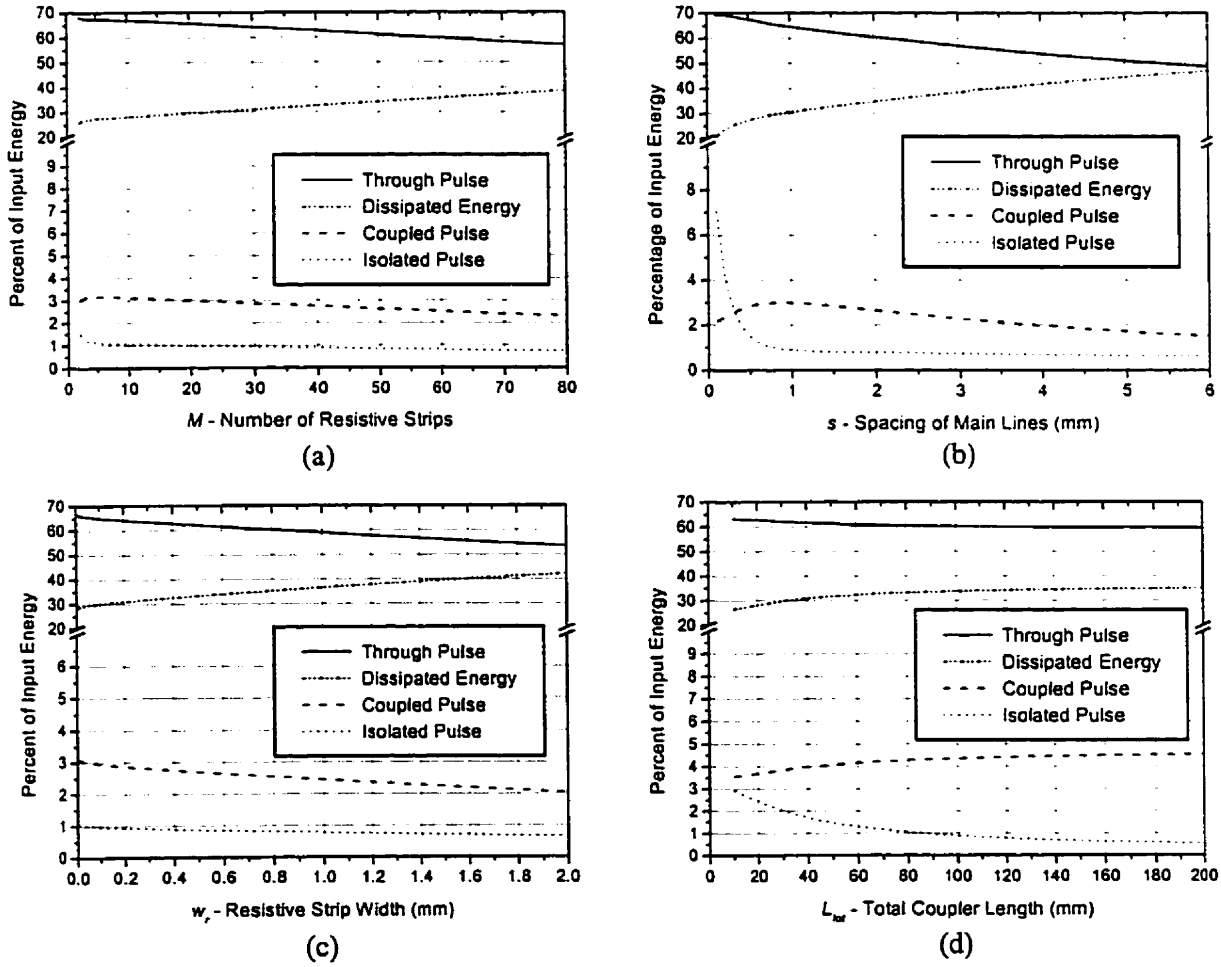

Figure 4-6. Effects of M, s, w_r, and L_{tot} on the dissipated energy of the coupler.

value of the parameter increases. In particular, it is important to keep s and w_r small, as they have the greatest effects on the dissipated energy. On the other hand, L_{tot} has quite a small effect on the dissipated energy, as there is only a 10% increase for this case. This allows a greater degree of freedom to use longer lengths in the coupler design.

4.2.2. Microstrip Considerations

Up to this point in the guidelines it has been assumed that the structure is operating in a homogeneous medium, so it is important to examine the differences for the inhomogeneous medium of microstrip. The primary difference, which was first discussed in Section 2.1.4.2, is the fact that the even and odd mode phase velocities are no longer equal. For this case, the forward EM coupling becomes stronger as L_{tot} increases, which inhibits the ability to use long coupler lengths to achieve good levels of directivity. This is because, the unwanted EM forward coupling leads to severe distortion of the coupled pulse, as is illustrated in Fig. 4-7. The solid lines in both graphs show how a stripline RDC with a total length of 100 mm performs in terms of coupling in the forward direction. If the same design is implemented in a microstrip form the coupled pulse would appear as the one shown in Fig. 4-7(b). The high frequency

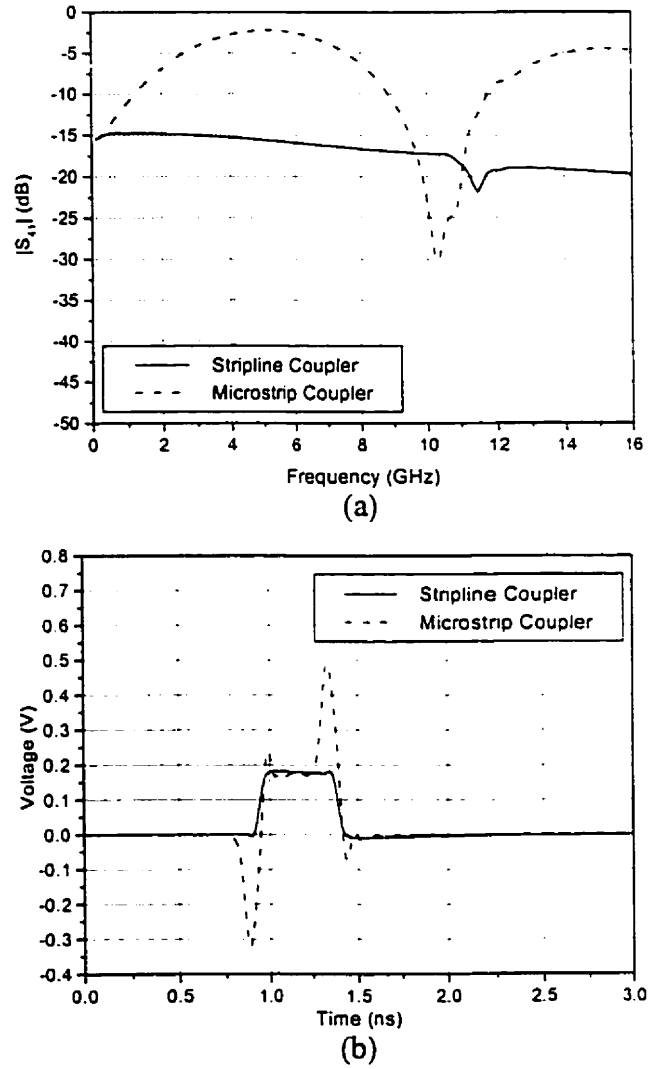

Figure 4-7. The $|S_{41}|$ characteristics and the forward coupled pulses for identical microstrip and stripline couplers.

components overpower the flat top of the pulse. It can be noted from Fig. 4-7(a) that for the an RDC, the forward coupling no longer reaches 0 dB due to portion of energy dissipated in the resistive strips.

These results show how difficult it is to design a microstrip RDC. Without the ability to use long lengths, the maximum achievable directivity is decreased and the range of possible couplings that can be synthesized is consequently reduced.

4.3. Design Procedure

With a thorough understanding of how the various design parameters effect the desired objectives, it is possible to easily synthesize RDCs given a set of specifications. The general design procedure is presented in the flow chart shown in Fig. 4-8.

From the desired coupler characteristic impedance Z_0, and depending on the substrate being used, the width of the main lines w can be determined. For this calculation, an educated guess can be made for s to find Z_0. However, due to the fact that the EM coupling will usually be quite small, the value of Z_0 will change very little when s is optimized later.

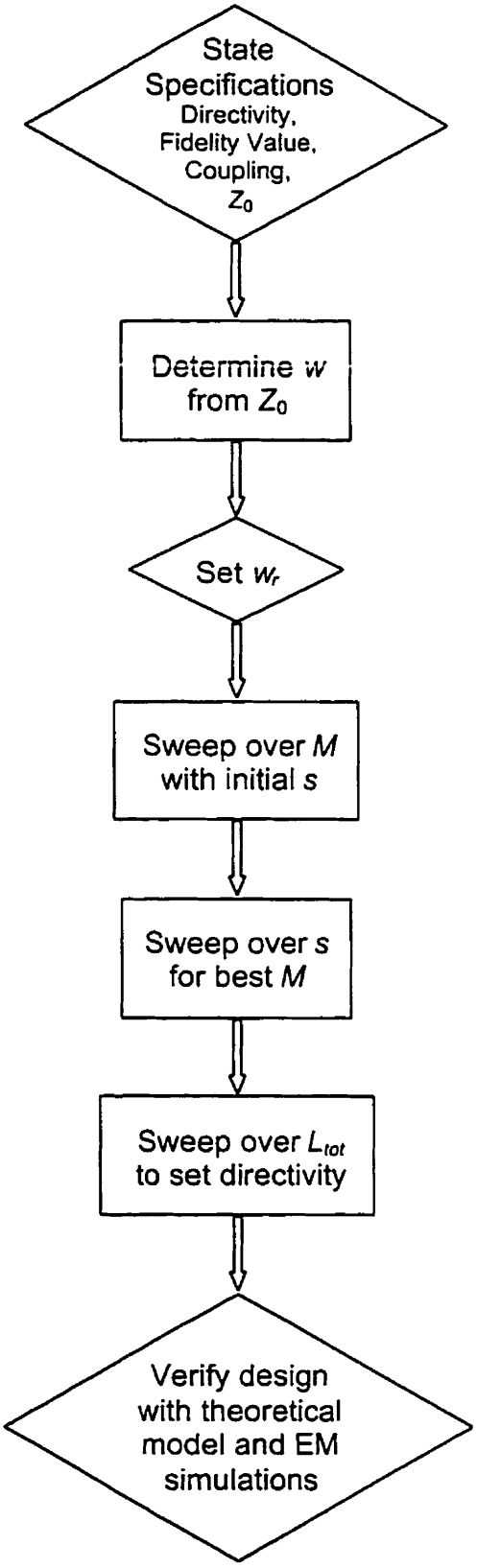

Figure 4-8. Design procedure for an RDC.

The next step is to decide upon a reasonable value for w_r, considering the limitations of the manufacturing process as well as the fact that for pulse fidelity and dissipated energy w_r should be kept as small as possible. With this value of w_r, it is possible to then sweep over a range of values for M using the estimate made for s above, as well as an estimate for the total length L_{tot}, both of which will be optimized later. From this sweep, the M value that provides the desired performance, e.g., maximum directivity, can then be used to sweep over a range of values for s. Once the value of s is set, then R_{so} can be determined from the desired level of coupling by using (4-5) and (4-8). If this value is not physically realizable, then w_r should be adjusted to reach a reasonable value for the sheet resistivity. Finally, since the value of L_{tot} only significantly affects the directivity, it can be set such that the specified directivity is obtained.

4.4. Resistive Directional Coupler Designs

Using the general guidelines described above designs for both stripline and microstrip environments were synthesized. An initial design was developed and then the theoretical model was used to optimize the design parameters. The theoretical performance of the final design was then validated against results obtained by the two EM simulators.

4.4.1. Stripline Couplers

As outlined above the even and odd modes in a stripline environment travel at the same velocity. This means that no matter how long the coupler is there will never be complete forward EM coupling. This permits longer coupler designs, which can improve the directivity while maintaining a flat $|S_{41}|$ response. Therefore, a stripline design can minimize the tradeoff between directivity and fidelity. For example, in designs where strong coupling to port #4 is desired, i.e., $|S_{41}|$ is large (>-15 dB), there is more freedom in the design due to

the relaxation on the need to suppress $|S_{31}|$ to achieve good directivity. However, for weak coupling designs there are greater restrictions on the design parameters.

4.4.1.1. 20 dB Coupler

The first stripline RDC design that will be presented is one in which the output pulse at port #4 contains only 1% of the energy of the input pulse. The coupler's design parameters are presented in Table 4-3, and its topology is similar to the one shown in Fig. 1-3, but the resistive strips are uniformly spaced.

Table 4-3 Design Parameters for the 20 dB Stripline RDC

w main line width	b plate spacing	s main line spacing	ε_r dielectric constant	w_r resistive strip width	R_{so} sheet resistance	M number of strips	L_{tot} total length
0.24 mm	1.27 mm	1.5 mm	9.8	0.0375 mm	50 Ω/sq	10	110 mm

The frequency-domain results for this coupler are shown in Fig. 4-9. The results obtained from the theoretical model match up very well with the simulated results. It can be seen that $|S_{31}|$ starts out at its DC value of -20 dB and then drops down to between -40 dB and -45 dB, which is the strength of the EM coupling given in Table 4-2 for these dimensions. The forward coupling parameter, $|S_{41}|$, drops off quite quickly with frequency, and this is a result of the reasonably large s value. However, both $|S_{41}|$ and $|S_{21}|$ stay constant enough over the frequency range of interest to produce good pulse fidelity.

The sharp resonances observed in each of the S-parameters occur at frequencies that correspond to the strip-to-strip spacing, L_1, being a multiple of a half-wavelength. At these frequencies, the signals travelling in the backward direction on the coupled line reinforce each other at port #3. This results in the notches seen in $|S_{41}|$ and the peaks observed in $|S_{31}|$. The peaks in $|S_{11}|$ are due to the addition at port #1 of the reflections from the main line to strip connections.

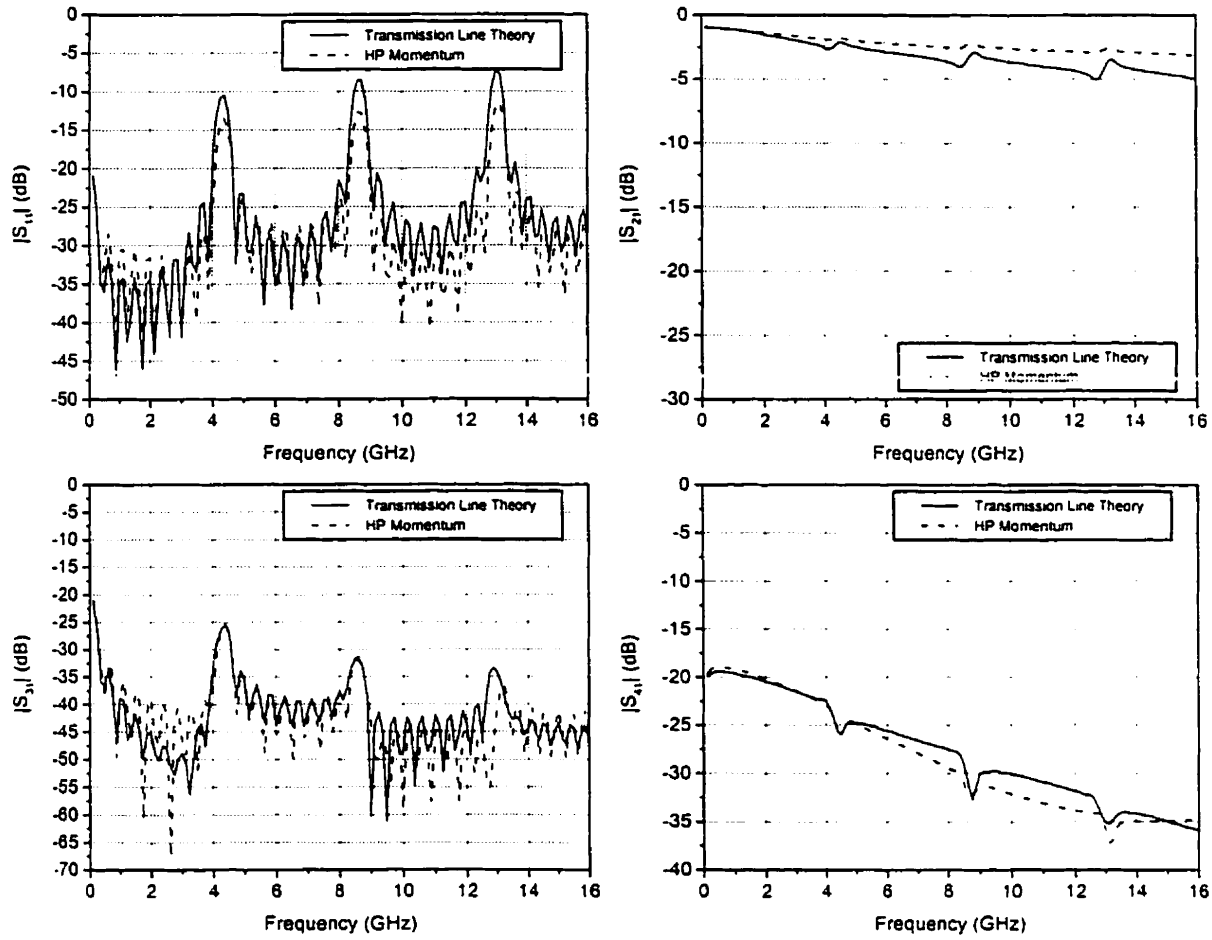

Figure 4-9. S-parameters for the 20 dB stripline coupler.

As will be shown in the next coupler design, it is possible to eliminate these resonances by spacing the strips non-uniformly along the coupler, as is shown in Fig. 1-3. However, it has been found that these designs result in lower directivities because the average values of $|S_{31}|$ and $|S_{11}|$ over the frequency range are larger than when the strips are uniformly spaced.

The time-domain results for this coupler are shown in Fig. 4-10. Included with each pulse is the percentage of the input energy that is contained within that pulse. The amount of dissipated energy and the coupler's directivity are also presented in the graphs.

Both of the pulses at ports #4 and #2 are good representations of the input pulse, while the signals at ports #1 and #3 are severely distorted versions of the input pulse. The losses for this design are fairly small due to the high impedances of the resistive strips which are required for weak coupling. This allows the through signal at port #2 to be large enough that it could continue on to other devices in a digital system.

The reflected signal is plotted with respect to the axis of the input pulse so that a proper comparison can be made. It is clear that for subsequent incoming pulses the reflections would be negligible. For the isolated signal, it is also small enough that if it were completely

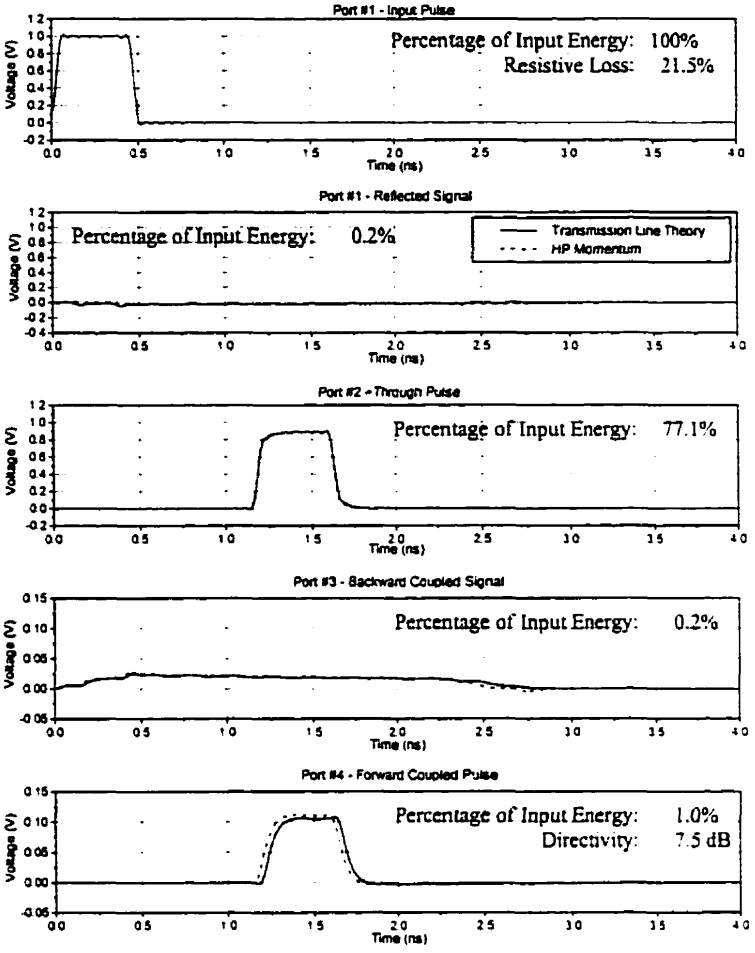

Figure 4-10. Time-domain response for the 20 dB stripline coupler.

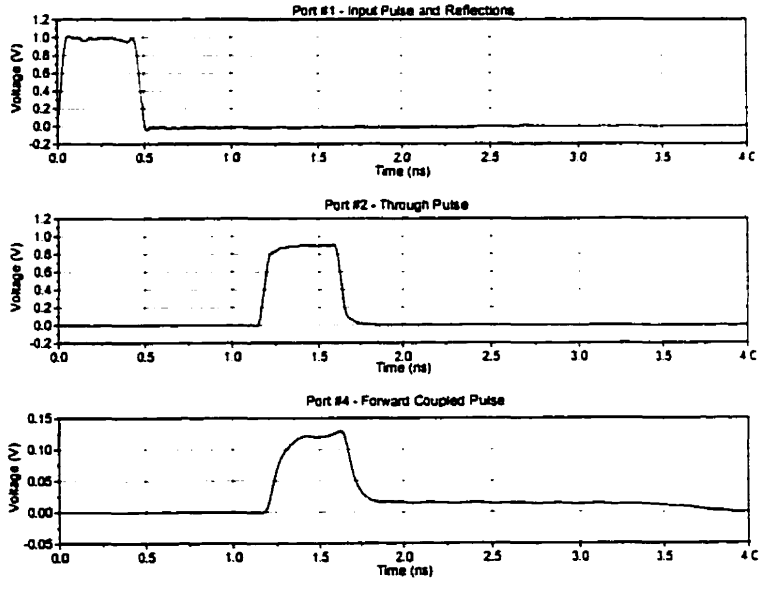

Figure 4-11. Time-domain response for 20 dB stripline coupler with port #3 left open-circuited.

reflected from port #3, i.e., port #3 was left open circuited, it would not interfere much with the forward coupled pulse. To show this, the time-domain simulations were recalculated with port #3 left open circuited. These results are shown in Fig. 4-11, and it is clear that port #3 could be left unterminated without any serious pulse degradations.

4.4.1.2. 11 dB Coupler

The goals of the second stripline design are to provide stronger coupling to port #4 with excellent pulse fidelity. The coupler uses non-uniformly spaced strips as well as a small main line spacing *s* to provide the pulse fidelity, with the consequence being a reduction in the maximum achievable directivity. However, this coupler will be designed for the shorter

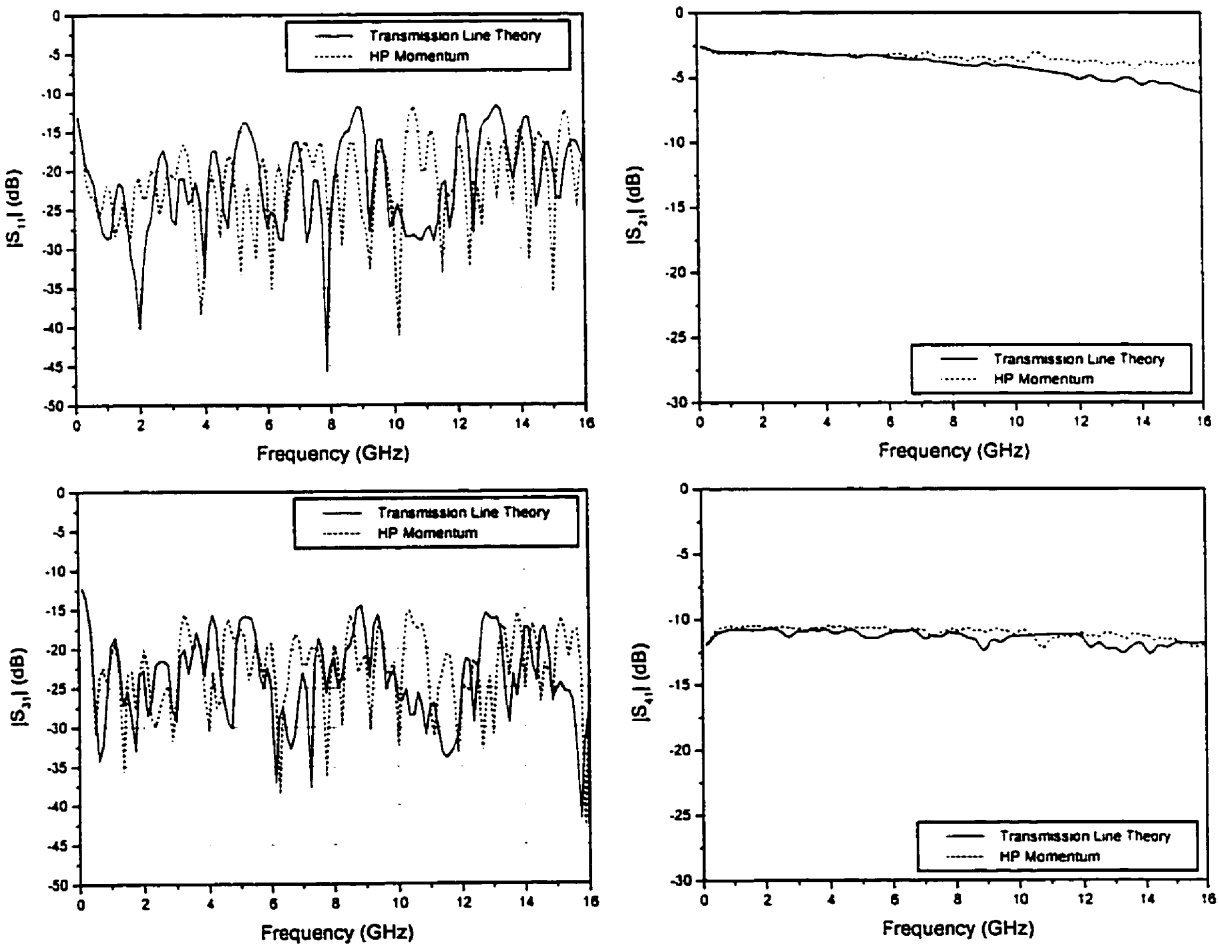

Figure 4-12. S-parameters for the 11 dB stripline coupler.

pulse, as shown in Fig. 3-5(b), which will allow a very good directivity to still be obtained. The parameters for this design are outlined in Table 4-4. The spacing of the resistive strips follow a linear profile, starting at 20 mm, decreasing with each strip by 4.5 mm to 2 mm, and then increasing by 4.5 mm back to 20 mm.

Table 4-4 Design Parameters for the 11 dB Stripline RDC

w main line width	b plate spacing	s main line spacing	ε_r dielectric constant	w_r resistive strip width	R_{so} sheet resistance	M number of strips	L_{tot} total length
0.24 mm	1.27 mm	0.6 mm	9.8	0.06 mm	50 Ω/sq	10	110 mm
Non-uniform resistive strip spacing: 20 mm → 2 mm → 20 mm							

The coupler's frequency response is shown in Fig. 4-12, while its time-domain performance is shown in Fig. 4-13. The directivity is very good, partly due to the use of the shorter pulse, and partly due to the fact that the strong DC coupling allows the freedom of placing the main lines closer together. As can be seen from Fig. 4-12, this closer spacing resulted in a much flatter $|S_{41}|$ and $|S_{21}|$ than was observed with the previous coupler.

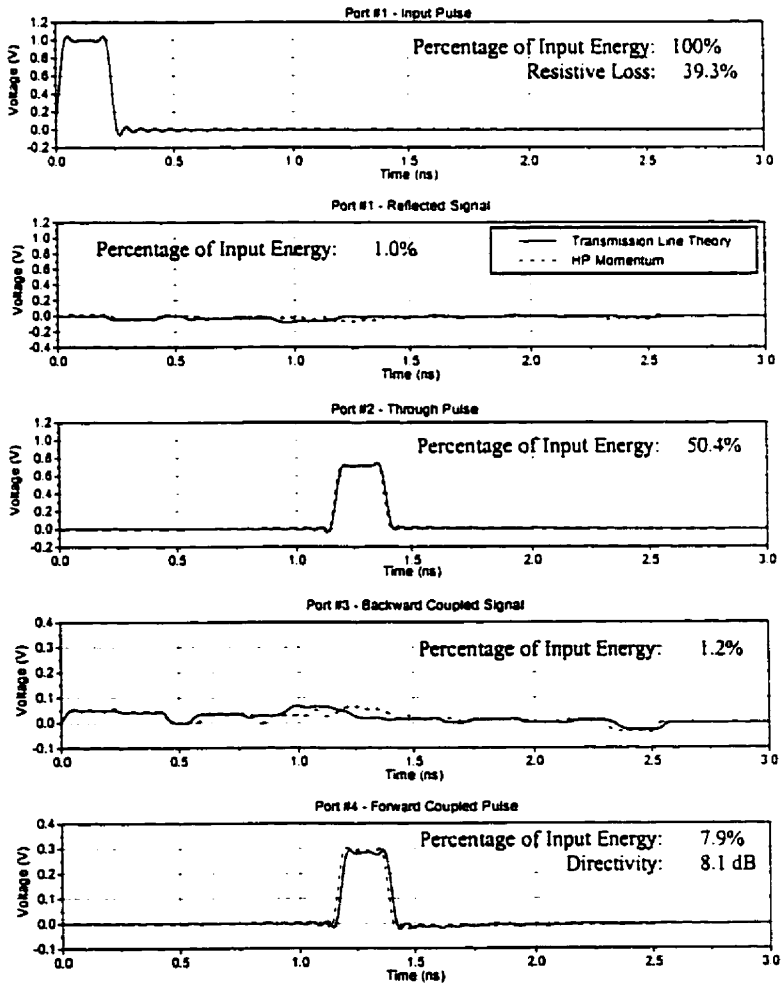

Figure 4-13. Time-domain response for the 11 dB stripline coupler.

4.4.2. Microstrip Couplers

As was discussed above, microstrip couplers are much more difficult to design due to the unwanted forward EM coupling. However, with the addition of the resistive strips to the coupled microstrip lines the coupling in the forward direction no longer reaches 0 dB due to the losses in the resistive strips. Therefore, by increasing these losses, the maximum EM coupling can be reduced. The design of this type of coupler becomes a matter of equalizing the EM forward coupling and the DC coupling to produce a $|S_{41}|$ profile that is as flat as possible. However, in practice it is quite difficult to completely flatten out the $|S_{41}|$ response.

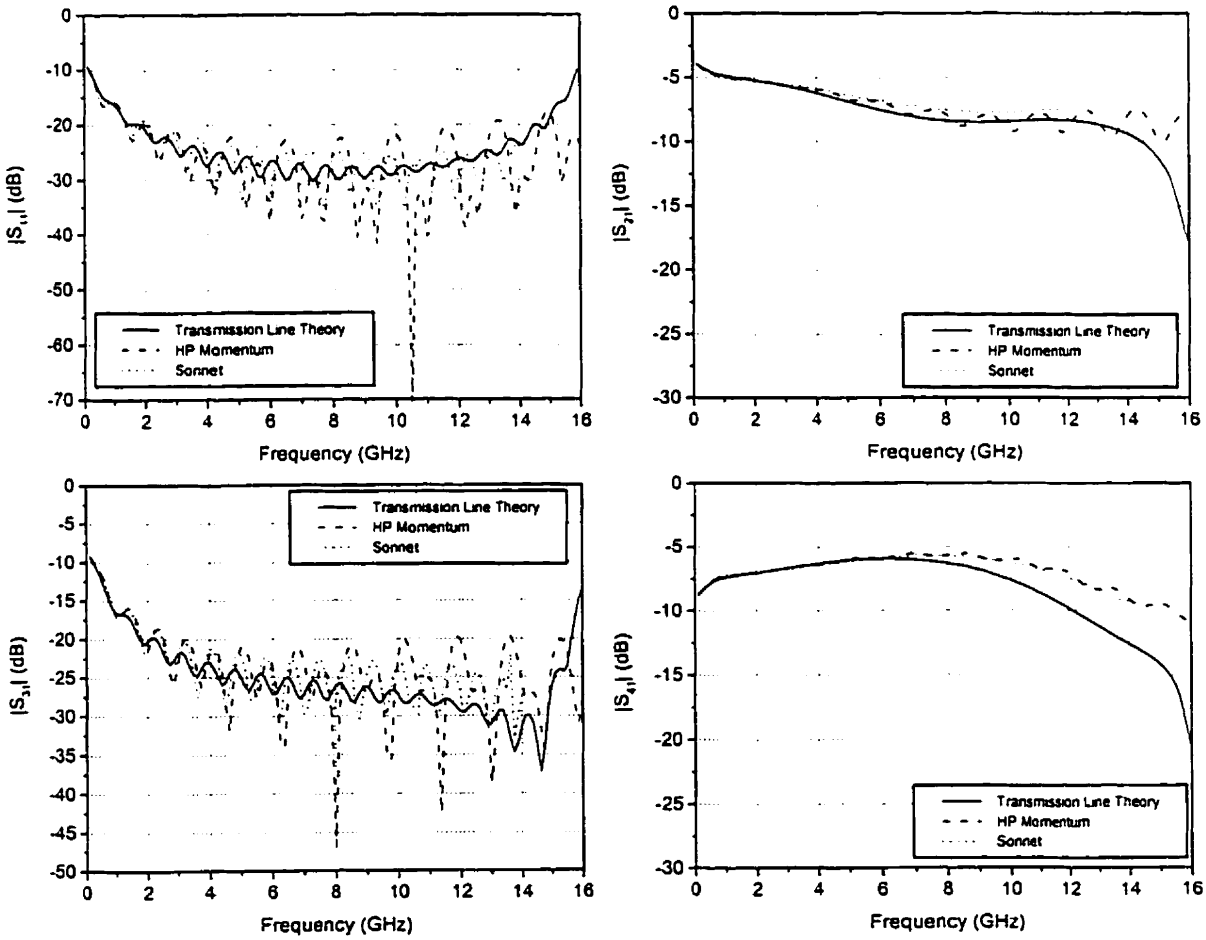

Figure 4-14. S-parameters for the 8 dB microstrip coupler.

Table 4-5 Design Parameters for the 8 dB Microstrip RDC

w	h	s	ε_r	w_r	R_{so}	M	L_{tot}
0.6 mm	0.635 mm	0.93 mm	9.8	0.116 mm	50 Ω/sq	20	63 mm

4.4.2.1. 8 dB Coupler

A strongly coupled microstrip RDC with uniform strip spacing was designed and has the design parameters outlined in Table 4-5. The S-parameter results are shown in Fig. 4-14. It can be seen that both $|S_{11}|$ and $|S_{31}|$ gradually drop to oscillate around -25 dB. The increases in $|S_{11}|$ and $|S_{31}|$ at higher frequencies are not critical when compared with the frequency spectrum of the digital pulses discussed in Section 3.3.1. Both $|S_{41}|$ and $|S_{21}|$ are relatively flat over the frequency range of interest. However, the effect of the forward EM coupling can be seen by the rise of $|S_{41}|$ in the middle of the frequency band.

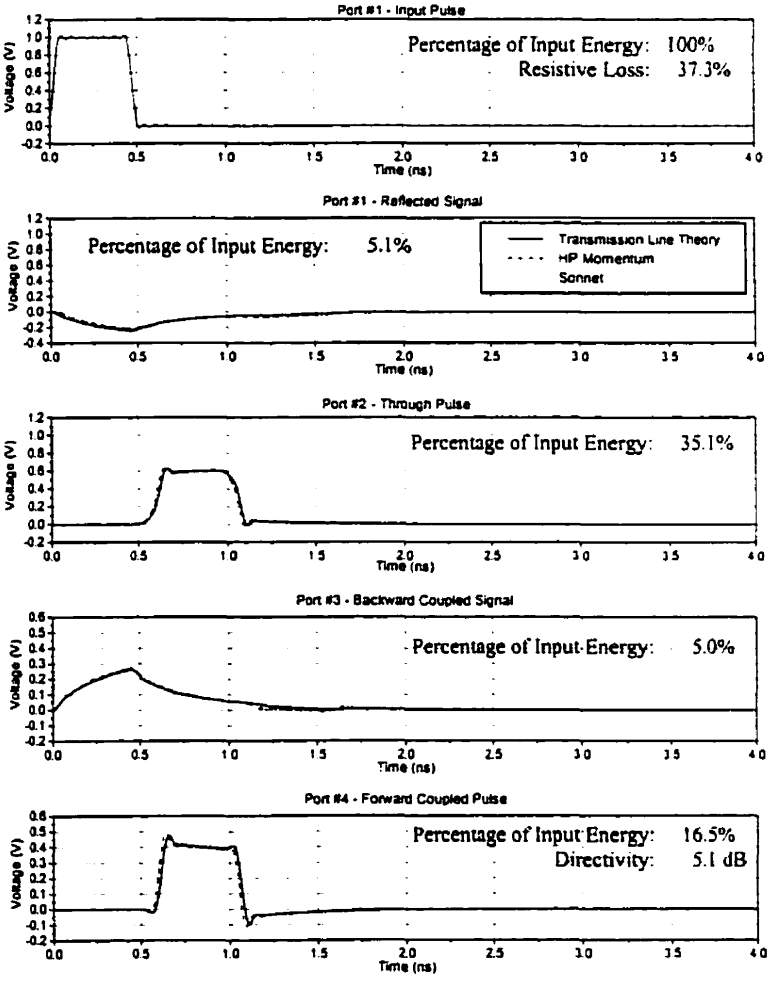

Figure 4-15. Time-domain response for the 8 dB microstrip coupler.

The output pulses at the four ports are shown in Fig. 4-15. The pulses appearing at ports #4 and #2 are good representations of the input pulse. Although, the pulses at ports #1 and #3 still have large amplitudes despite the fact that they are significantly distorted.

Chapter 5

FUTURE WORK AND CONCLUSIONS

5.1. Future Work

5.1.1. Isolated Port Terminations

It was found that in order to achieve good isolation at port #3, a long coupler length was required. In these cases, and especially for the stripline couplers, the signal that appeared at port #3 was small enough that this port could be left open-circuited. However, if port #3 could be properly terminated without the use of vias or wrap-around straps then the need for long couplers could be minimized resulting in couplers with more reasonable lengths for common use.

In [18], Buoli presented an open-circuited resistive termination that could provide a real input impedance over a wide range of frequencies. This real input impedance was created by periodically loading a length of resistive transmission line with open-circuited resistive stubs. Since a resistive material is already being used in the RDC, this may be an excellent way of terminating port #3. Preliminary studies have shown that the signal can be attenuated by such a termination, but further study is needed to prove its feasibility.

5.1.2. Phase Velocity Compensation for Microstrip RDCs

The difference between the even and odd mode phase velocities in a microstrip edge-to-edge coupler was shown to have caused a degradation in the coupler's performance. The idea of equalizing these two modal velocities to improve the directivity has been a popular topic of study for many researchers. The general concept is to alter the coupler design in such a way that only the odd mode is affected, thus slowing it down. One of the simplest

ways of doing this is to place a capacitive element between the two coupled lines. This has been shown to achieve a large improvement in the directivity [23].

A more popular way of velocity equalization is to introduce a wiggle or a saw-tooth profile along the inner edges of the two lines. This method has been well researched and documented [24] and is preferred due to the fact that it can be implemented using planar manufacturing techniques only.

With further research, these methods could also be applied to the microstrip RDC. This would allow a greater variety of attainable coupling levels and could vastly improve the coupler's directional characteristics.

5.2. Conclusions

The review of the coupling theory illustrated the mechanisms that led to backward and forward coupling in parallel-coupled lines. It was later observed that both of these mechanisms were present in an RDC, and that both of them had to be considered in the design process to achieve the desired coupler characteristics.

The methods of analysis of an RDC design for both the frequency and time domains were introduced. The theoretical model that was derived is more general than the previously published model. The present model can analyze coupler designs made up of individual cells, meaning the cell length or the strip contained within the cell could vary along the coupler. This model was validated for a number of coupler designs using two commercially available EM simulators.

With the ability to rapidly analyze coupler designs using the theoretical model, a design procedure for an RDC was developed. It was based on the theoretical fundamentals of the coupler and the effects of each of the design parameters on the fidelity, directivity, and

the loss characteristics of the coupler. This procedure was used to design two stripline couplers with different coupling levels and fidelity values. The major drawback of these designs was the total length needed to produce the high levels of directivity. A microstrip coupler design was also presented that improved upon the directivity of the design presented by Jenkins and Cullen. However, it has been observed that the forward EM coupling in the microstrip environment greatly reduces the flexibility of the RDC design procedure.

REFERENCES

[1] L. Young, Ed., *Parallel Coupled Lines and Directional Couplers*, Dedham, Massachusetts: Artech House, 1972.

[2] S. V. Robertson, A. R. Brown, L. P. B. Katehi, and G. M. Rebeiz, "A 10-60 GHz micromachined directional coupler," *IEEE Trans. Microwave Theory and Tech.*, vol. MTT-46. 1998. pp. 1845-1849.

[3] A. Jenkins and A. L. Cullen, "Resistive four-port directional coupler," *IEE Proc.*, vol. 129, pp. 94-98, 1982.

[4] R. E. Matick, *Transmission Lines for Digital and Communication Networks*. New York: IEEE, 1995, pp. 268-309.

[5] M. K. Krage and G. I. Haddad, "Characteristics of coupled microstrip transmission lines – I: Coupled-mode formulation of inhomogeneous lines," *IEEE Trans. Microwave Theory and Tech.*, vol. MTT-18, pp. 217-222, 1970.

[6] J. E. Adair and G. I. Haddad, "Coupled-mode analysis of nonuniform coupled transmission lines," *IEEE Trans. Microwave Theory and Tech.*, vol. MTT-17, pp.746-752, 1969.

[7] E. G. Cristal, "Coupled-transmission-line directional couplers with coupled lines of unequal characteristic impedances," *IEEE Trans. Microwave Theory and Tech.*, vol. MTT-14, pp. 337-346, 1966.

[8] S. B. Cohn, "Characteristic impedance of the shielded-strip transmission line," *IRE Trans. Microwave Theory and Tech.*, vol. MTT-2, pp. 52-57, 1954.

[9] B. M. Oliver, "Directional electromagnetic couplers," *Proc. IRE*, vol. 42, pp. 1686-1692, 1954.

[10] Gupta, et. al., *Microstrip Lines and Slotlines*, Boston: Artech House, 1996.

[11] P. K. Ikäläinen and G. L. Matthaei, "Wide-band, forward-coupling microstrip hybrids with high directivity," *IEEE Trans. Microwave Theory and Tech.*, vol. MTT-35, pp. 719-725, 1987.

[12] R. Levy, "Directional couplers," in *Advances in Microwaves*, vol. 1, L. Young, Ed. New York: Academic Press, 1966.

[13] T. G. Bryant and J. A. Weiss, "Parameters of microstrip transmission lines and of coupled pairs of microstrip lines," *IEEE Trans. Microwave Theory and Tech.*, vol. MTT-16, pp. 1021-1027, 1968.

[14] S. Deibele and J. B. Bayer, "Measurement of microstrip effective relative permittivities", *IEEE Trans. Microwave Theory and Tech.*, vol. MTT-35, pp. 535-538, 1987.

[15] M. Kirschning and R. H. Jansen, "Accurate wide-range design equations for the frequency-dependent characteristic of parallel coupled microstrip lines," *IEEE Trans. Microwave Theory and Tech.*, vol. MTT-32, pp. 83-90, 1984.

[16] S. B. Cohn, "Shielded coupled-strip transmission line," *IRE Trans. Microwave Theory and Tech.*, vol. MTT-3, pp. 29-38, 1955.

[17] H. A. Wheeler, "Formulas for the skin effect," *Proc. IRE*, vol. 30, 1942, pp. 412-424, 1942.

[18] C. Buoli, "Microstrip attenuators and terminations realized with periodic electromagnetic structures," in *Proc. 18th European Microwave Conf.*, Tunbridge Wells, 1988, pp. 593-598.

[19] Sonnet Software Documentation, *EM User's Guide*, Chapter 1 – Introduction, 1998.

[20] W. L. Stutzman and G. A. Thiele, *Antenna Theory and Design*, New York: John Wiley & Sons, 1981, pp. 306-332.

[21] HP – Momentum Documetation, *Momentum User's Guide*, Chapter 9 – Theory of Operation, 1995.

[22] C. D. McGillem and G. R. Cooper, *Continuous and discrete signal and system analysis*, 3rd ed. Philadelphia: Saunders College Pub., 1991.

[23] D. Kaifez, "Raise coupler directivity with lumped compensation," *Microwaves*, vol. 17, pp. 64-65, 68-70, 1978.

[24] S. Uysal, *Nonuniform Line Microstrip Directional Couplers and Filter*, Boston: Artech House, 1993.